Available online at www.sciencedirect.com
SCIENCE DIRECT®
Geochimica et Cosmochimica Acta 70 (2006) 1402–1420
Geochimica
www.elsevier.com/locate/gca

# Albite dissolution kinetics as a function of distance from equilibrium: Implications for natural feldspar weathering

Mikala S. Beig *, Andreas Lüttge

*Department of Earth Science—MS 126, Rice University, P.O. Box 1892, Houston, TX 77251-1892, USA*

Received 31 January 2005; accepted in revised form 24 October 2005

**Abstract**

Determining the kinetics of many geologic and engineering processes involving solid/fluid interactions requires a fundamental understanding of the Gibbs free energy dependency of the system. Currently, significant discrepancies seem to exist between kinetic datasets measured to determine the relationship between dissolution rate and Gibbs free energy. To identify the causes of these discrepancies, we have combined vertical scanning interferometry, atomic force microscopy, and scanning electron microscopy techniques to identify dissolution mechanisms and quantify dissolution rates of albite single crystals over a range of Gibbs free energy ($-61.1 < \Delta G < -10.2$ kJ/mol). During our experiments, both a previously dissolved albite surface exhibiting etch pits and a pristine surface lacking dissolution features were dissolved simultaneously within a hydrothermal, flow-through reactor. Experimental results document an up to 2 orders of magnitude difference in dissolution rate between the differently pretreated surfaces, which are dominated by different dissolution mechanisms. The rate difference, which persists over a range of solution saturation state, indicates that the dissolution mechanisms obey different Gibbs free energy dependencies. We propose that this difference in rates is the direct consequence of a kinetic change in dissolution mechanism with deviation from equilibrium conditions. The existence of this kinetic "switch" indicates that a single, continuous function describing the relationship between dissolution rate and Gibbs free energy may be insufficient. Finally, we discuss some of the potential consequences of our findings on albite's weathering rates with a particular focus on the sample's history.


## 1. Introduction

Many kinetic processes of critical environmental importance occur close to thermodynamic equilibrium, and derive their driving force from relatively small free energy differences (Pačes, 1972, 1973; Merino, 1975; Gíslason and Arnórsson, 1990; White and Brantley, 2003). However, many of these processes are difficult to explore at near-equilibrium conditions in laboratory experiments. Far-from-equilibrium, feldspar dissolution kinetics have been studied extensively in the past resulting in a substantial database of dissolution rates. Most studies have employed flow-through reactors containing a mineral powder and have focused on the dependence of dissolution rates on a single parameter such as pH, temperature, concentration of inorganic cations, and dislocation density (e.g., Holdren and Berner, 1979; Chou and Wollast, 1984, 1985; Helgeson et al., 1984; Holdren and Speyer, 1985a,b, 1987; Knauss and Wolery, 1986; Brantley et al., 1986; Brantley and Stillings, 1996; Mast and Drever, 1987; Amrhein and Suarez, 1988, 1992; Casey et al., 1988a,b; Talman and Nesbitt, 1988; Cygan et al., 1989; Murphy, 1989; Schweda, 1989; Oxburgh et al., 1994; Stillings and Brantley, 1995; Stillings et al., 1996; Stoessel and Pittman, 1990; White and Peterson, 1990; Muir and Nesbitt, 1991; Nesbitt et al., 1991; Rose, 1991; Huang and Longo, 1992; Ganor et al., 1995). The overall dissolution rates measured during these experiments were derived from changes in solution chemistry. Because of the difficulty of acquiring data close to equilibrium investigators have attempted to extrapolate the far-from-equilibrium data to near-equilibrium conditions. However, results often have been dissatisfactory because a successful extrapolation requires a fundamental

* Corresponding author.
*E-mail address:* mbeig@alumni.rice.edu (M.S. Beig).

0016-7037/$ - see front matter © 2005 Elsevier Inc. All rights reserved.
doi:10.1016/j.gca.2005.10.035

understanding of the dependence of dissolution rate on the Gibbs free energy of the dissolution reaction. To develop this understanding, a handful of investigators have measured dissolution rates of minerals such as gibbsite, kaolinite, smectite, labradorite, and albite over a range of Gibbs free energies approaching equilibrium conditions (e.g., Nagy et al., 1991; Nagy and Lasaga, 1992; Burch et al., 1993; Gautier et al., 1994; Oelkers et al., 1994; Devidal et al., 1997; Oelkers and Schott, 1999; Taylor et al., 2000; Berger et al., 2002). While internally consistent, comparison of the datasets collected by different investigators reveals fundamental differences in the measured dependence of rate on distance from equilibrium. As an example, Fig. 1 shows four sets of rate data plotted as a function of $\Delta G$: (i) Data for albite and labradorite (Figs. 1A and B) measured by Burch et al. (1993) and Taylor et al. (2000) both are compatible with a sigmoidal relationship between dissolution rate and saturation state. Rates that are measured sufficiently far from equilibrium become independent of $\Delta G$ establishing the so-called *dissolution plateau*. As equilibrium is approached the dissolution rates decrease sharply over a small range of Gibbs free energy. Close to equilibrium the curve is approximately linear with a shallow slope and rates approaching zero. (ii) Data for albite and potassium feldspar (Figs. 1C and D, Oelkers et al., 1994 and Gautier et al., 1994; respectively), in contrast, show a linear relationship with dissolution rates decreasing steadily as equilibrium is approached. It is interesting that the latter authors do not find a dissolution plateau where the dissolution rate becomes finally independent of $\Delta G$. Currently, the discrepancies between datasets raise questions as to the true nature of the relationship(s) between dissolution rate and Gibbs free energy and prevent us from extrapolating the large database of far-from-equilibrium

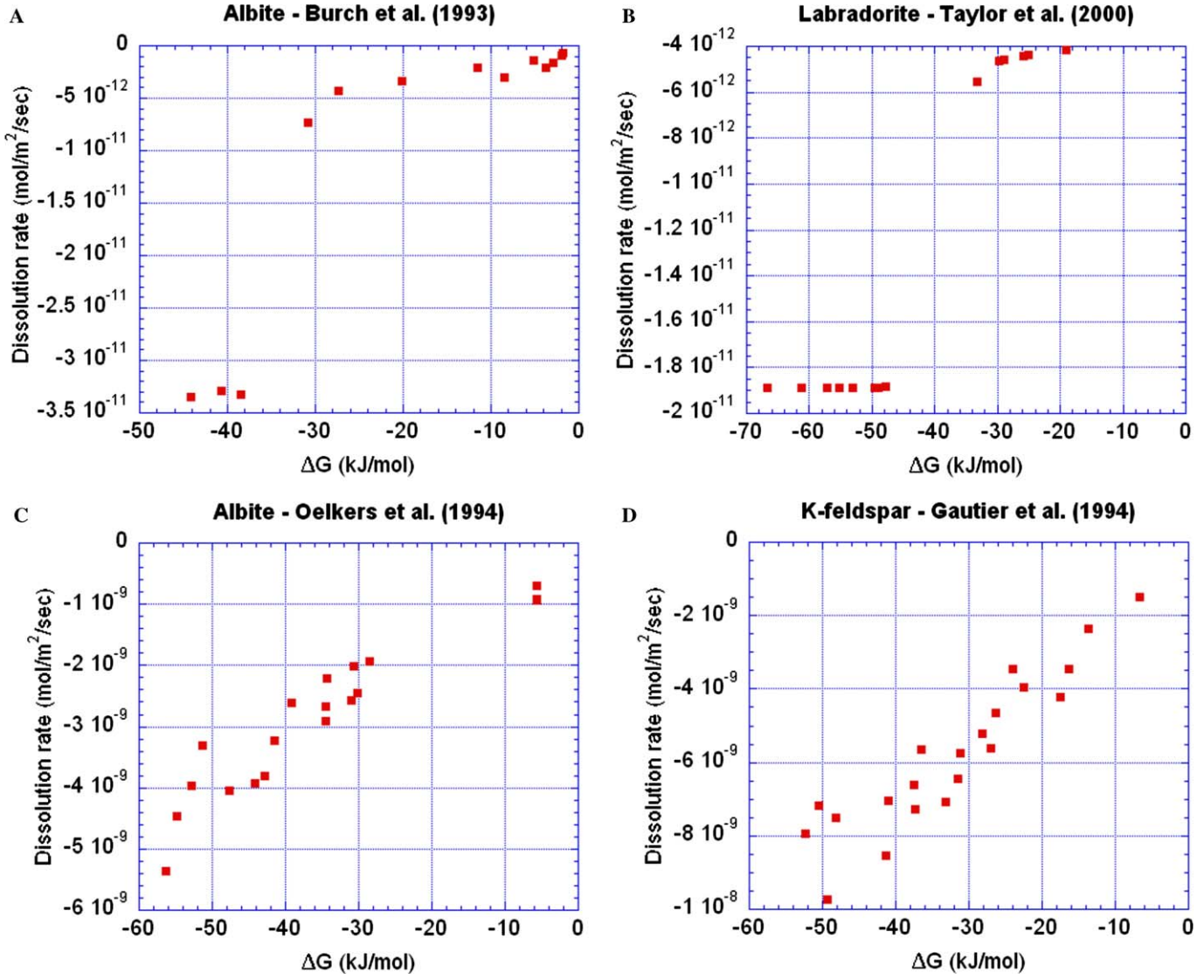


Fig. 1. Dissolution rate versus Gibbs free energy for a variety of feldspar minerals. (A) Albite, pH 9 and 80 °C (Burch et al., 1993). (B) Labradorite, pH 3 and 25 °C (Taylor et al., 2000). (C) Albite, pH 9 and 150 °C (Oelkers et al., 1994). (D) Potassium feldspar, pH 9 and 150 °C (Gautier et al., 1994). Note the distinct differences in the distribution of data between the top two and bottom two datasets.

rates to near-equilibrium geologic and engineering problems.

It has long been recognized that etch pits play an important role in the dissolution process (Berner and Holdren, 1979; Berner and Schott, 1982; Helgeson et al., 1984; MacInnis and Brantley, 1992, 1993; Frank, 1951; Burton et al., 1951; Cabrera et al., 1954; Cabrera and Levine, 1956; Lasaga, 1998; Lasaga and Blum, 1986; Tang and Nancollas, 2000; Lasaga and Lüttge, 2001, 2003; Tang et al., 2001, 2003; Brantley et al., 1986; Nagy and Lasaga, 1992; Burch et al., 1993; Taylor et al., 2000). Lasaga and Lüttge (2001, 2003) introduced their "dissolution stepwave model" to describe the relationship between etch pit formation, Gibbs free energy, and dissolution rate. Their model is based upon the observation that etch pits contribute to the total dissolution rate not only by the localized removal of material, but also by the generation of steps away from the center of the pits. These steps, called "dissolution stepwaves," remove layer after layer of material resulting in an overall reduction of the crystal surface. When etch pits are present, dissolution rates are enhanced. When etch pits are absent, dissolution is limited to existing surface features, such as the steps resulting from cleaving or grinding. Derived in the context of BCF theory (BCF, Burton, Cabrera, and Frank, see below) and also postulated by the stepwave model, a critical Gibbs free energy, $\Delta G_{crit}$, must be achieved for pits to open. Based on these considerations, we can envision two different scenarios illustrated in Fig. 2. The schematic dashed lines represent rates controlled by dissolution at steps on a relatively flat surface in the absence of etch pits. The solid lines represent rates that are enhanced by the presence of etch pits. In this context, we hypothesize that two mineral surfaces with different histories can yield significantly different dissolution rates when reacted at the same Gibbs free energy.

To test this hypothesis we dissolved two albite crystals with different histories under identical environmental conditions and compared their dissolution rates and mechanisms. We employed a combination of vertical scanning interferometry (VSI) and atomic force microscopy (AFM) for investigating the dynamics of dissolving cleavage surfaces. We build upon previous work during which the microtopography of albite surfaces was examined before and after dissolution using AFM (Hochella et al., 1990; Drake and Hellmann, 1991; Hellmann et al., 1992). The current study quantifies albite single-crystal dissolution rates based upon observations of changes in surface topography during dissolution, i.e., the physical surface-normal retreat of the dissolving crystal face. The complementary use of VSI and AFM instrumentation allows us to observe the crystal surface directly and to identify the ways in which rates and dissolution mechanisms respond to changes in solution chemistry. This approach has been tested successfully before during anorthite and calcite dissolution experiments (Lüttge et al., 1999; Arvidson et al., 2005; Vinson and Lüttge, 2005). The results of the current study offer an intriguing potential explanation for the apparent discrep-

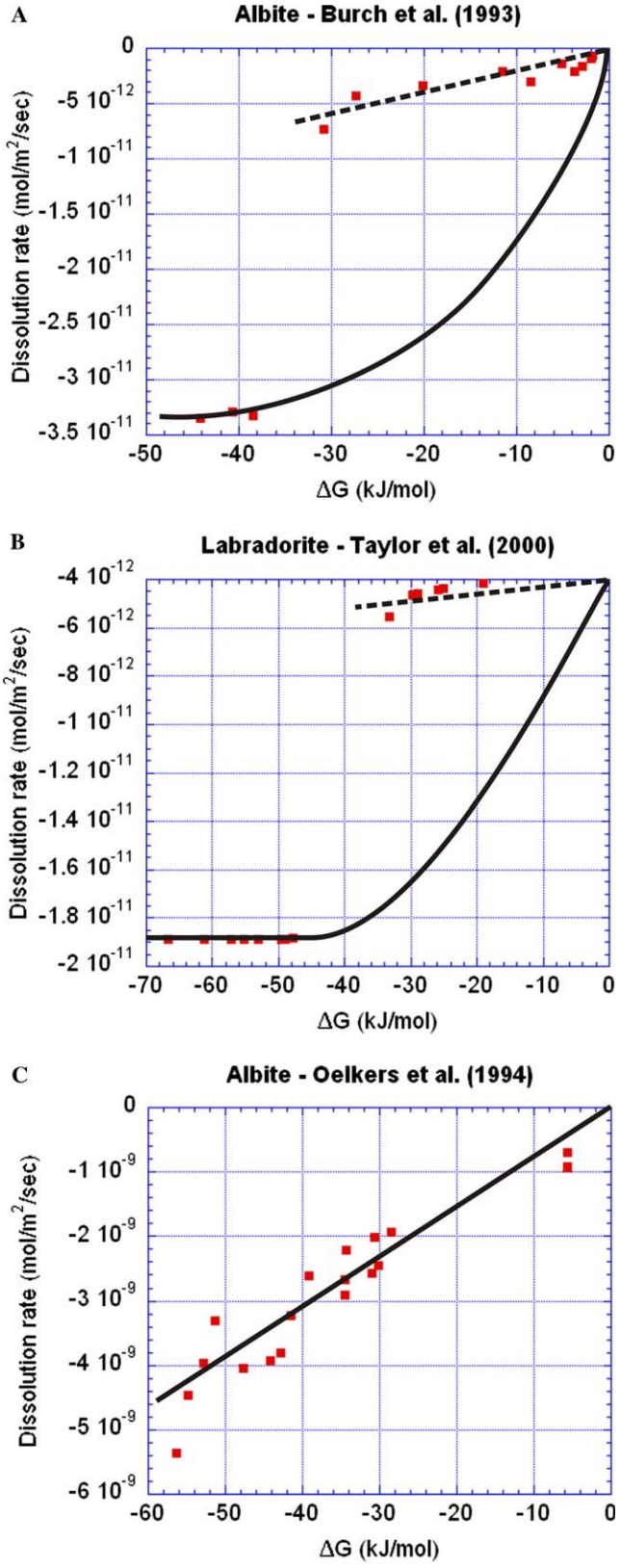


Fig. 2. Schematic curves representing the Gibbs free energy dependencies of the pit-free (dashed lines) and pit-dominated (solid lines) mechanisms. The lines have been drawn over the dissolution rate data of (A) Burch et al. (1993), (B) Taylor et al. (2000), and (C) Oelkers et al. (1994). The rate data in (A) and (B) exhibit a kinetic bifurcation with deviation from equilibrium. The data in (C) are best fit with a single, continuous function for the relationship between dissolution rate and Gibbs free energy.

ancies between existing dissolution rate versus Gibbs free energy datasets and contribute to the ongoing discussion (e.g., Hellmann and Tisserand, 2006).

## 2. Materials and methods

Our initial experiments (Table 1) were aimed at determining the environmental conditions necessary for monitoring dissolution rates on single crystals of albite on a reasonable laboratory time scale using VSI. Subsequent experiments (Table 2) focused on quantifying dissolution rates on albite cleavage surfaces over a range in Gibbs free energy at 185 °C and pH 9. The dissolution experiments summarized in Table 1 were conducted with freshly cleaved crystals. The dissolution experiments summarized in Table 2 were conducted with both a pre-etched and a freshly cleaved crystal dissolving simultaneously within the same reactor (Table 2). The pretreatment consisted of reaction at pH 9, 185 °C, and $\Delta G_r < -35$ kJ/mol. We will refer to all pre-etched crystal surfaces as "treated" and freshly cleaved crystal surfaces as "untreated." The topographies and dissolution rates of the "treated" and "untreated" cleavage surfaces were compared post-reaction.

### 2.1. Materials

During the experiments detailed herein, we used albite from two locales: Amelia Courthouse, Virginia and Therison, West Crete, Greece (Seidel, 1978; Seidel et al., 1982). The Amelia albite occurs in a pegmatite. The Greek albite

Table 1
Temperature-dependence experiments

| Experiment | Locale | hkl | Temperature (°C) | pH | $\Delta G$ (kJ/mol) | Flow rate (ml/min) | Duration (h) | Surface normal retreat rate (mol/m$^2$/s) | Etch pit volume rate (mol/m$^2$/s) | Relative uncertainty rate (%) |
|---|---|---|---|---|---|---|---|---|---|---|
| ab no 1 | Virginia | (010) | 25 | 3 | [a] | 3.6 | 593.75 | 0 | 0 | na |
| ab no 2 | Virginia | (010) | 80 | 3 | [a] | 3.6 | 154 | 0 | 0 | na |
| grab02 | Greece | (001) | 25 | 3 | [a] | 3.6 | 960 | 0 | $1.7\times10^{-19}$ | 22 |
| grab22 | Greece | (001) | 80 | 9 | [a] | 3.6 | 624 | 0 | 0 | na |
| ab01-1 | Virginia | (010) | 150 | 9 | −48.5[c] | 3.0 | 119.62 | $5.4\times10^{-10}$ | [b] | 5 |
| ab03_A | Greece | (001) | 200 | 9 | [a] | 3.0 | 67.5 | $4.8\times10^{-8}$ | [b] | 4 |
| ab03_D | Greece | (001) | 200 | 9 | [a] | 3.0 | 26.25 | $1.0\times10^{-8}$ | [b] | 14 |

[a] Gibbs free energy data unavailable. Single crystals only, no powder.
[b] No separate measurement necessary when a surface normal retreat is measured.
[c] Al and Si in solution due to powder dissolution in reactor.

Table 2
Gibbs free energy dependence experiments

| Experiment | Pretreated | Average $\Delta G$ (kJ/mol) | Flow rate (ml/min) | Duration (h) | Surface normal retreat rate (mol/m$^2$/s) | Etch pit volume rate (mol/m$^2$/s) | Relative uncertainty rate (%) | Etch pit density (pit/μm$^2$) |
|---|---|---|---|---|---|---|---|---|
| ab12A | Yes | −61.1[b] | 0.35 | 75.27 | $1.4\times10^{-8}$ | [d] | 6 | [e] |
| ab12B | No | −61.1[b] | 0.35 | 75.27 | $1.4\times10^{-8}$ | [d] | 3 | [e] |
| ab05A1 | No | [a,b] | 0.30 | 25.75 | $2.2\times10^{-9}$ | [d] | 17 | [e] |
| ab07B1 | No | −55.0[b] | 0.30 | 45.83 | $6.8\times10^{-9}$ | [d] | 6 | [e] |
| ab09A1 | No | −52.0[b] | 0.30 | 42.07 | $6.0\times10^{-9}$ | [d] | 3 | [e] |
| ab10A1 | No | −35.1[c] | 0.30 | 76.12 | $1.7\times10^{-9}$ | [d] | 12 | [e] |
| ab13A2 | Yes | −29.3[c] | 0.35 | 138.53 | $4.9\times10^{-9}$ | [d] | 7 | [e] |
| ab13B | No | −29.3[c] | 0.35 | 138.53 | $1.3\times10^{-9}$ | [d] | 6 | [e] |
| ab10A2 | Yes | −25.9[c] | 0.25 | 167.38 | $1.2\times10^{-9}$ | [d] | 11 | [e] |
| ab10B | No | −25.9[c] | 0.25 | 167.38 | $9.2\times10^{-10}$ | [d] | 26 | 0.034 |
| ab08A2 | Yes | −20.5[c] | 0.60 | 91.82 | $1.6\times10^{-9}$ | [d] | 15 | 0.038 |
| ab08B | No | −20.5[c] | 0.60 | 91.82 | $6.8\times10^{-10}$ | [d] | 22 | 0.085 |
| ab09A2 | Yes | −14.5[c] | 0.56 | 98.80 | $2.2\times10^{-9}$ | [d] | 12 | [e] |
| ab09B | No | −14.5[c] | 0.56 | 98.80 | 0 | $5.9\times10^{-11}$ | 20 | 0.021 |
| ab06A2 | Yes | −12.3[c] | 0.26 | 143.50 | $2.9\times10^{-9}$ | [d] | 3 | [e] |
| ab06B | No | −12.3[c] | 0.26 | 143.50 | 0 | $2.0\times10^{-11}$ | 15 | 0.021 |
| ab05A2 | Yes | −10.9[c] | 0.26 | 148.75 | 0 | $5.4\times10^{-10}$ | 22 | [e] |
| ab05B | No | −10.9[c] | 0.26 | 148.75 | 0 | $8.0\times10^{-11}$ | 25 | 0.022 |
| ab11B | No | −10.2[c] | 0.30 | 121.55 | 0 | $5.3\times10^{-12}$ | 12 | 0.041 |

Greek Albite, (001) cleavage surface, pH 9, 185 °C.
[a] Gibbs free energy unavailable. Assumed to be similar to following two experiments due to similar experimental conditions.
[b] Saturation state set by albite single crystal dissolution.
[c] Saturation state set by albite powder dissolution.
[d] No separate measurement necessary when surface normal retreat is measured.
[e] Not measured due to significant pit coalescence.

occurs in cracks in alkali-basaltic metavolcanites. Both samples had EDS electron microprobe based compositions of $Ab_{99.8}$ (CAMECA SX-50, Rice University). Single crystals were cleaved and flat surfaces approximately $5 \times 5$ mm were obtained. Samples were then ultrasonically cleaned in water to remove fine particles. The crystallographic orientation of the cleavage surfaces was verified with X-ray diffraction (Rigaku DMAX-2000, CuK$\alpha$ radiation). Because the Amelia albite is platy and cleaves more readily along (010), dissolution experiments employing Amelia albite single crystals were conducted on the (010) cleavage surface. Albite twinning, which is expressed on the (001) cleavage surfaces, did not affect the dissolution rates measured on the (010) surfaces. Single crystals of the Greek albite show perfect cleavage on (001), thus dissolution experiments employing the Greek albite were conducted on the (001) cleavage surface. The Greek albite exhibited macroscale ($\sim$1 cm) twinning, which was expressed on the (001) cleavage surfaces. All dissolution rates were measured in between twin planes. Examination of the twin plane boundaries post-reaction did not reveal enhanced dissolution. Because of its near-gem quality and mirror-like cleavage surfaces, all of the experiments summarized in Table 2 were conducted using single crystals of the Greek albite.

A portion of the Amelia albite was handpicked and subsequently ground under methanol with an agate mortar and pestle. The resulting powder was then sieved to isolate particular grain size fractions. To achieve a solution with a free energy of dissolution with respect to albite ($\Delta G_r$) greater than or equal to $-35.1$ kJ/mol (see footnotes in Table 2), the albite powder was dissolved in the reactor along with the single crystals. A smaller grain size fraction (e.g., 20–45 μm) was used to achieve solution chemistries with $\Delta G_r \geqslant -25.9$ kJ/mol. The 75–106 μm grain size fraction was used to achieve solution chemistries with $-29.3$ kJ/mol $\geqslant \Delta G_r \geqslant -35.1$ kJ/mol. As initially fast powder dissolution rates were desired, no attempt was made to eliminate ultrafine particles by washing the mineral powder. An initially high concentration of Al and Si released into solution insures that the saturation state of the fluid within the reactor, and in contact with the single crystals, is not further from equilibrium than the target saturation state for the experiment. An additional safeguard against negative deviations in equilibrium was implemented during experiments at $\Delta G_r \geqslant -29.3$ kJ/mol. Upon assembly, the dissolution reactor was filled with a room temperature "starter" solution containing sufficient concentrations of Si and Al to achieve the desired $\Delta G_r$ at 185 °C. To mitigate the precipitation of possible secondary phases this solution was mixed immediately before the start of each experiment. Each starter solution contained stoichiometric (with respect to albite) concentrations of Si and Al (by dissolving sodium metasilicate and aluminum chloride). In contrast, the input solution that was pumped into the reactor for the duration of the experiment contained no Si and Al. Once the starter solution had exited the reactor after a residence time of approximately 5.5 h, the desired $\Delta G_r$ value was achieved solely by the dissolution of the single albite crystals and powder within the reactor.

The initial experiments (Table 1) were conducted at pH 3 and 9, and varying temperature (25–200 °C). The low-pH experiments were conducted in 0.001 M HCl. Basic solutions were buffered to pH 9 with 0.01 M sodium tetraborate. All subsequent experiments (Table 2) were conducted at pH 9 in order to avoid complications related to the nucleation of secondary phases (analcime, gibbsite, kaolinite, and boehmite) as equilibrium with respect to albite was approached. The pH of input solutions was measured at room temperature using a semi-micro combination electrode with a Corning 450 pH/ion meter. The pH of solutions within the reactor at temperatures >25 °C was calculated during the saturation state calculations. Solutions were sparged with nitrogen to eliminate dissolved $CO_2$.

### 2.2. Solution saturation states

Solution saturation states for experiments conducted at temperatures $\leqslant$80 °C were not determined. During the experiments conducted at temperatures $\geqslant$150 °C two methods were used to achieve the desired solution saturation state. First, experiments conducted at Gibbs free energies $<-50$ kJ/mol contained single crystals only and the solution saturation state was determined by the contribution of constituent ions from the dissolving single crystal. Second, experiments conducted at $\Delta G > -50$ kJ/mol contained a mineral powder in addition to the single crystals and the solution saturation state was determined by the contribution of constituent ions from both the dissolving powder and single crystals. An example of the solution chemistry to which Greek albite single crystals were exposed during experiments employing an albite powder is given in Fig. 3. Because of the enormous difference in surface area between the single crystals and finely ground powders, we assume that the solution chemistry was dominated by the powder signature. Independent electron microprobe analyses of Amelia albite yielded Si:Al stoichiometries of 2.7, 3.0, and 3.1 (Harlow and Brown, 1980; Hellmann, 1994). The solutions during experiments conducted at $\Delta G_r \geqslant -29.3$ kJ/mol were considered to be stoichiometric with respect to the albite. During the experiments conducted at $\Delta G_r \leqslant -35.1$ the Si:Al ratios ranged from 1.5 to 2.5 indicating enrichment in Al.

The saturation state in the reactor was verified by monitoring Si and Al concentrations in effluent samples. Si and Al concentrations were analyzed colorimetrically immediately upon collection (Varian Cary 50 UV–visible, Rice University) using the heteropoly blue and catechol violet methods (APHA Standard Methods, 1995 and Dougan and Wilson, 1974), respectively. Relative uncertainties for the Si and Al measurements were 4% and 9%, respectively. The free energies of dissolution, defined as $\Delta G_r = RT\ln(Q/K_{eq})$, were calculated using the EQ3NR speciation/solubility code (Wolery, 1983) based upon the reaction:

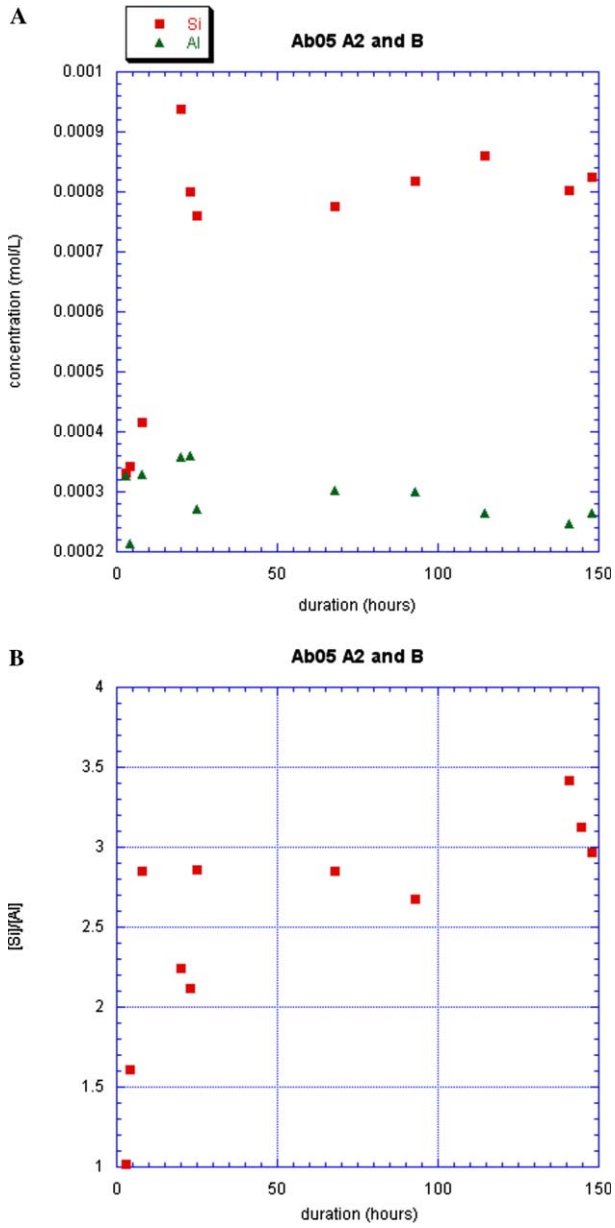


Fig. 3. Solution chemistry data from the experiment conducted at pH 9, 185 °C, and $\Delta G_r = -10.9$ kJ/mol. (A) Si and Al concentrations over time. (B) Si:Al ratios over time.

$$NaAlSi_3O_8 + 4H^+ \leftrightarrow 2H_2O + Al^{3+} + Na^+ + 3SiO_2(aq) \quad (1)$$

### 2.3. Reactor descriptions

Experiments conducted at temperatures $\leqslant$80 °C employed an acrylic flow through cell (wetted volume 1.5 ml) equipped with PEEK fittings and Teflon tubing. Samples were mounted on the ends of titanium rods and inserted into the flow-through cells so that the top of the single-crystals were level with the flow path of the incoming fluid. One port of the fluid cell accommodated a thermocouple, which was connected to a temperature controller to maintain the water bath at a constant temperature (±1 °C). The other two ports accommodated the inlet and outlet fittings and tubing. Solutions were stored in HDPE Nalgene bottles and were non-recycling. During the lower temperature experiments a two-component epoxy was applied over small areas (1 mm diameter) of the single-crystal surface. The surface area under the epoxy was protected from reaction and served as a reference surface for measurements of surface normal retreat after dissolution (Lüttge et al., 1999). The epoxy was easily removed and did not affect the mineral surface beneath.

Experiments conducted at temperatures 150–200 °C employed an experimental technique that combined the capabilities of a single-crystal and powder flow-through reactor (Arvidson et al., 2004). The titanium reactor (Fig. 4) was capable of housing both single-crystals and mineral powders and reacting them at temperatures ranging from 25

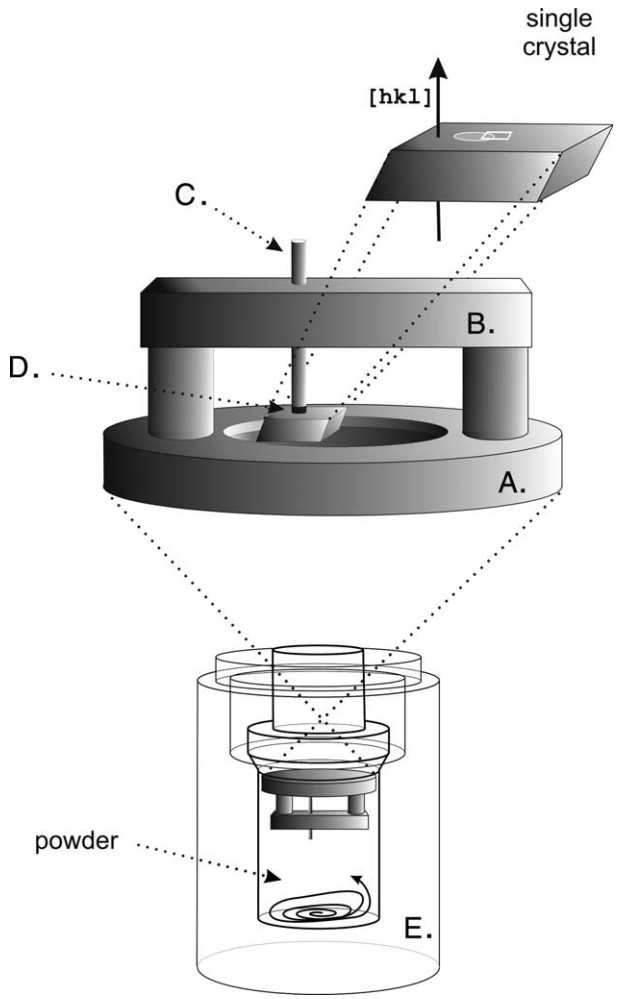


Fig. 4. Schematic of the titanium, hydrothermal, flow-through reactor used for the >80 °C experiments. Adapted from Fig. 1 in Arvidson et al. (2005). (A) Sample holder, (B) bridge, (C) threaded pin, (D) Viton mask, and (E) reactor body. A stir bar (not shown) is suspended from the bridge to ensure uniform mixing with the reactor. During experiments in which a mineral powder is used, the powder is loose within the reactor and is kept in motion by stirring.

to 250 °C. The wetted reactor volume was approximately 100 mL and housed a sample holder and stir bar assembly. A detailed description of the reactor assembly is given in Arvidson et al. (2004), and will be briefly summarized here.

An inverted sample holder was suspended inside the fluid from the cap of the reactor (Fig. 4A). A titanium disk with a shallow well served as the sample holder (~2 mm) on which single crystals were fixed with a thin film of high temperature, two-component epoxy. A "bridge" was fastened to the sample holder spanning the area on which the sample was fixed (Fig. 4B). This bridge held a threaded pin, which fixed a Dupont Viton nib (3 mm diameter) in place on the crystal surface (Fig. 4C). The nib served as a mask to prevent wetting of this portion of the crystal surface, as well as an anchor to hold the sample in place. The maximum temperature of the experiments was defined by the chemical stability of the fluoroelastomer (Dupont Viton) mask. The nib effectively protected an area of the mineral surface from reaction and provided the necessary reference for absolute height measurements. A stir bar suspended from the inverted sample holder and bridge assembly maintained a stirring rate of 100 rpm.

The temperature of the system was maintained by surrounding the reactor with a cylindrical, fused silica, 1050 W electric coil furnace attached to a temperature controller. A system back pressure of approximately 35 bar was maintained with a gas-loaded back pressure regulator. Fluid was supplied to the reactor at a constant flow rate by a Teledyne Isco high-pressure syringe pump. Solutions were stored in 10 L Nalgene carboys and were sparged with nitrogen before and during the 5 min pump refill period.

### 2.4. Dissolution rate measurements

As described above the protected area underneath the epoxy ($T \leqslant 80$ °C) or the Viton mask ($T > 80$ °C) served as a reference plateau from which to measure the surface-normal retreat of the mineral during the dissolution reaction (Figs. 5A and B). The development of the albite surface was monitored using VSI (ADE Phase Shift Technologies, Inc., MicroXAM MP-8, Rice University). Height data were collected with the interferometer and converted to topographic images with the Mapvue software (ADE Phase Shift Technologies, Inc.). For a detailed description

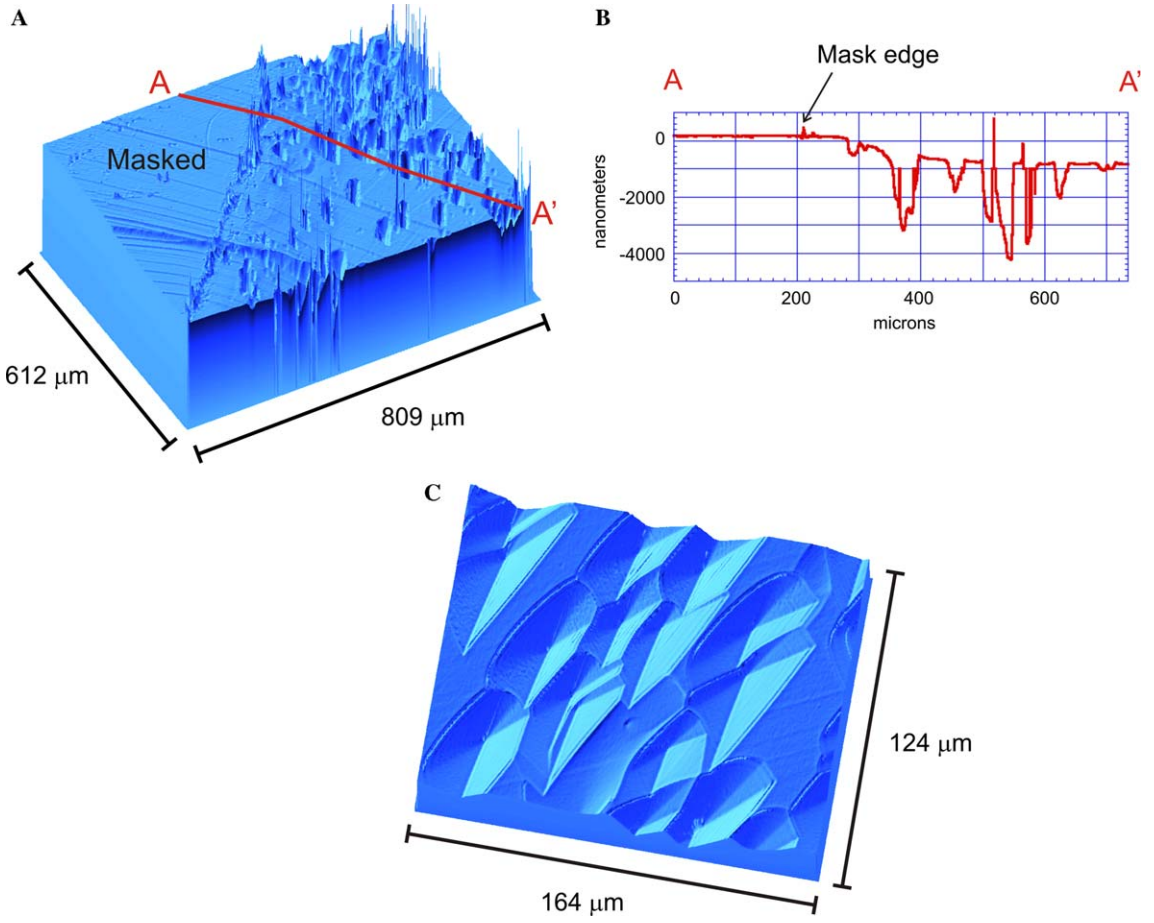


Fig. 5. (A) 3D topographic image (10×) of Greek albite (001) cleavage surface after 68 h of reaction at pH 9 and 200 °C. Masked area can be seen clearly. Reacted area is characterized by etch pits. (B) Line profile (A–A′) across reference plateau and reacted portions of the cleavage surface clearly shows surface normal retreat. (C) 3D topographic image (50×) of reacted area highlighting rhomb-shaped, pyramidal etch pit morphology.

of this interferometry technique see, e.g., Lüttge et al. (1999, 2003). All measurements were taken using a standard halogen white light source. Scans of up to 100 μm were possible with vertical resolution better than 2 nm and horizontal resolution of 500 nm. Height data were collected over scans 845 × 630 μm and 165 × 125 μm with 10× and 50× Mirau objectives, respectively. Measurements of the difference in height between the reference plateau and the reacted portion were taken after each dissolution experiment. A minimum of 20 profiles between the protected and reacted cleavage surfaces was taken per scan. An example of such a profile can be seen in Fig. 5. Approximately 5–10 scans (100–200 profiles) per cleavage surface were used for height measurements. The height differences measured from each profile were averaged. The development of the average height difference over time yielded a surface-normal retreat rate, which was divided by the molar volume of albite to obtain the dissolution rate in mol/m$^2$/s (Lüttge et al., 1999; Lüttge, 2004). In some cases multiple scans could be overlain to align matching surface features (Fig. 6). This "stitching" technique allowed us to characterize dissolution features over a larger field of view than provided by a single scan.

VSI dissolution rates with the lowest relative error are obtained when there is sufficient surface-normal retreat of the mineral surface with respect to the reference surface. On a perfectly flat surface, we can measure as little as 1 nm surface normal retreat. Natural cleavage surfaces, however, are rough in comparison. Ideally, the surface-normal retreat should be at least two times greater than the statistical range in height across the pristine surface in order to be measured easily and consistently. Because of extremely slow dissolution rates, during some experiments in this study the surface-normal retreat was not resolvable within the roughness of the mineral surface. In these cases only the albite volume removed by etch pit formation was measured, representing a minimum dissolution rate. Etch pit volumes were measured using the Mapvue software. The volume analysis calculates the total volume below a plane that is positioned by the investigator in a way that it intersects the flat terraces between etch pits. The resulting volume divided by the area of the image represents the mean depth of the pits. This value divided by the duration of the experiment and the molar volume of albite yields an etch pit based dissolution rate in moles per surface area per time (i.e., mol/m$^2$/s).

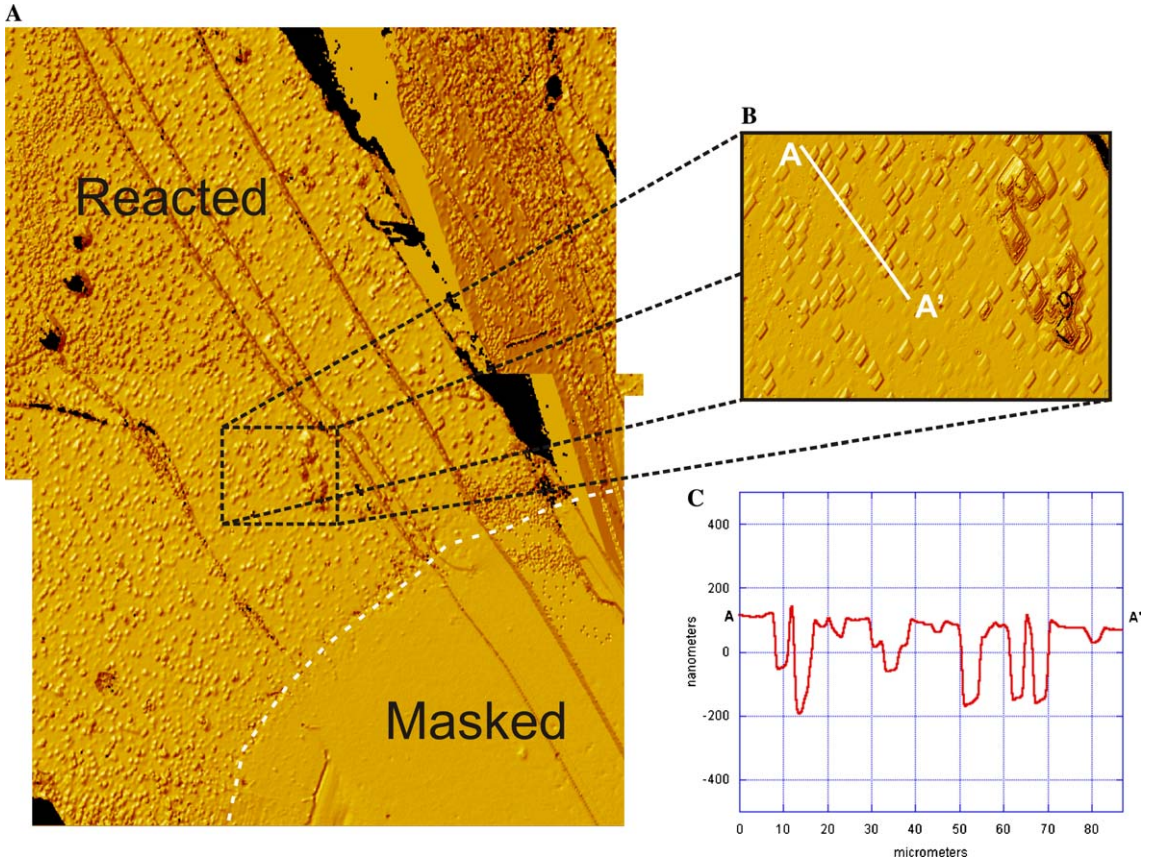


Fig. 6. (A) Topographic image of Greek albite (001) cleavage surface after 76 h of reaction at pH 9, 185 °C, and $\Delta G_r = -35.1$ kJ/mol. Two 10× images have been "stitched" together to increase the field of view. (B) 50× image of reacted portion of the cleavage surface illustrating rhomb-shaped etch pit morphology. Elongation perpendicular to the (010) cleavage direction indicates that the rate of movement of the "short" walls of etch pits is faster than the longer walls. (C) Line profile (A–A′) across reacted mineral surface highlighting etch pit dimensions.

### 2.5. Atomic force microscopy and scanning electron microscopy

For experiments conducted closer to equilibrium than $\Delta G_r = -12.3$ kJ/mol, the etch pits produced were too small for their morphologies to be resolved with the 50× Mirau objective. In these cases the crystal surfaces were studied by AFM and/or SEM. AFM imaging of mineral surfaces was conducted using a Molecular Imaging PicoSPM II 2500 (Rice University). All scans were performed ex situ in air using contact mode. With its large scanner this instrument was capable of scanning up to $80 \times 80$ μm.

SEM imaging of mineral surfaces was conducted with a JEOL JSM-840 scanning electron microscope using secondary electrons (Rice University). All crystal surfaces were sputter-coated with gold prior to imaging.

## 3. Results

### 3.1. Temperature dependency of albite dissolution rates

The results of the 25 and 80 °C experiments are presented in Table 1. No surface-normal retreat was measurable within the 1–2 nm resolution of the VSI in any of the four experiments. Based upon a maximum surface normal retreat of 1 nm and experimental durations of 154–960 h, the maximum possible dissolution rates of those surfaces ranged from $2.9 \times 10^{-17}$ to $1.8 \times 10^{-16}$ mol/m$^2$/s. Only one of the low temperature experiments produced VSI detectable etch pits (grab02—Table 1). Volume analysis of the etch pits yielded a dissolution rate of $1.71 \times 10^{-19}$ mol/m$^2$/s, significantly lower than the calculated maximum ($2.9 \times 10^{-17}$ mol/m$^2$/s for that experiment).

Results from a number of >80 °C experiments are also presented in Table 1. Increasing the experimental temperature increased dissolution rates dramatically. Etch pit development and surface normal retreat during the 200 °C experiments was significant (Table 1 and Fig. 5).

### 3.2. Gibbs free energy dependency of albite dissolution rates and mechanisms

#### 3.2.1. Dissolution rates

Fig. 7 summarizes the dissolution rates of the samples in Table 2 as a function of $\Delta G_r$. As expected, the dissolution rates of *untreated* crystals (squares) decreased with increasing $\Delta G_r$ but in a varying fashion. The dependence of dissolution rate on $\Delta G_r$ can be divided into three regions (Fig. 7). Region 1, which includes experiments conducted at $\Delta G_r > -18$ kJ/mol, is characterized by a linear dependence of rate on $\Delta G_r$ with a very shallow slope. Region 2, between −62 and −20 kJ/mol, was also characterized by a linear relationship, but with a stronger dependence of rate on $\Delta G_r$. In region 3, which included rates measured at $\Delta G_r \leqslant -52$ kJ/mol, rates exhibited the strongest dependence on $\Delta G_r$ The dissolution rate dependence on $\Delta G_r$ of the *pretreated* crystals (signature of triangles in Fig. 7)

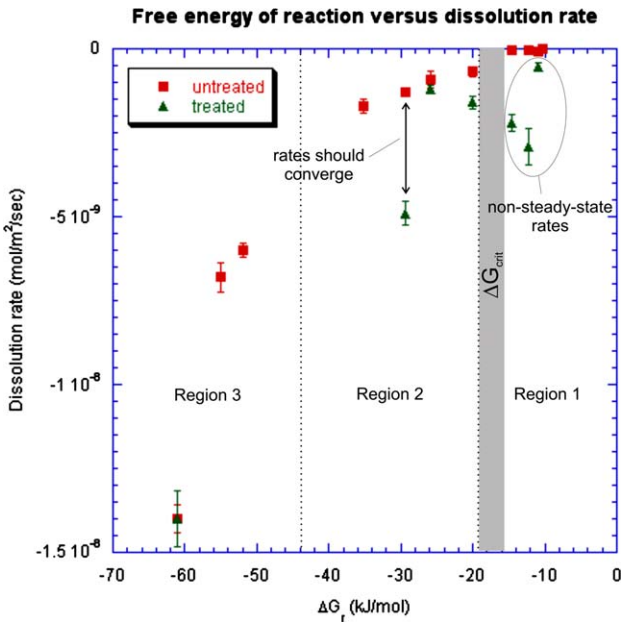


Fig. 7. Plot of rate data versus free energy of dissolution from experiments summarized in Table 2. All rates were measured on Greek albite single-crystals.

exhibited significantly more variation, but in general also decreased with approach to equilibrium.

The dissolution rate of these pretreated samples was 0.6–2 orders of magnitude *faster* than their pristine sample pairs (Fig. 7). For the experiment conducted at $\Delta G_r = -10.9$ kJ/mol, the difference in overall rate is a function of etch pit development, and is illustrated in the time series of Fig. 8. During pretreatment at far-from-equilibrium conditions, etch pits are formed rapidly on the surface (Fig. 8A). It is an important observation that during subsequent reaction, the volume change of these pits far exceeded the volume change of nascent pits forming on the pristine samples. An example of these volume differences is shown in Fig. 8: $2.8 \times 10^{10}$ nm$^3$ versus $3.4 \times 10^{8}$ nm$^3$ (cf. profiles A–A′ and B–B′). In this case, the differences in etch pit development corresponded to a ~7-fold difference in dissolution rates ($5.36 \times 10^{-10}$ versus $8.05 \times 10^{-11}$ mol/m$^2$/s). Other pretreated/pristine sample pairs showed similar differences in dissolution rates at the same $\Delta G_r$. For experiments at $\Delta G_r = -12.3$ and −14.5 kJ/mol, the differences in dissolution rates were a function of etch pit development on the non-pretreated surface and an overall surface normal retreat on the pretreated sample. For experiments at $\Delta G_r \leqslant -20.5$ kJ/mol, the differences in dissolution rates were a function of surface normal retreat on both samples. The relative uncertainties in dissolution rate listed in Table 2 are based upon the standard error of all rate measurements of a given sample.

#### 3.2.2. Etch pit densities

Cleavage surfaces reacted at $\Delta G_r \leqslant -20.5$ kJ/mol were examined using VSI. Cleavage surfaces reacted $\Delta G_r \geqslant -14.5$ kJ/mol were examined using either AFM or

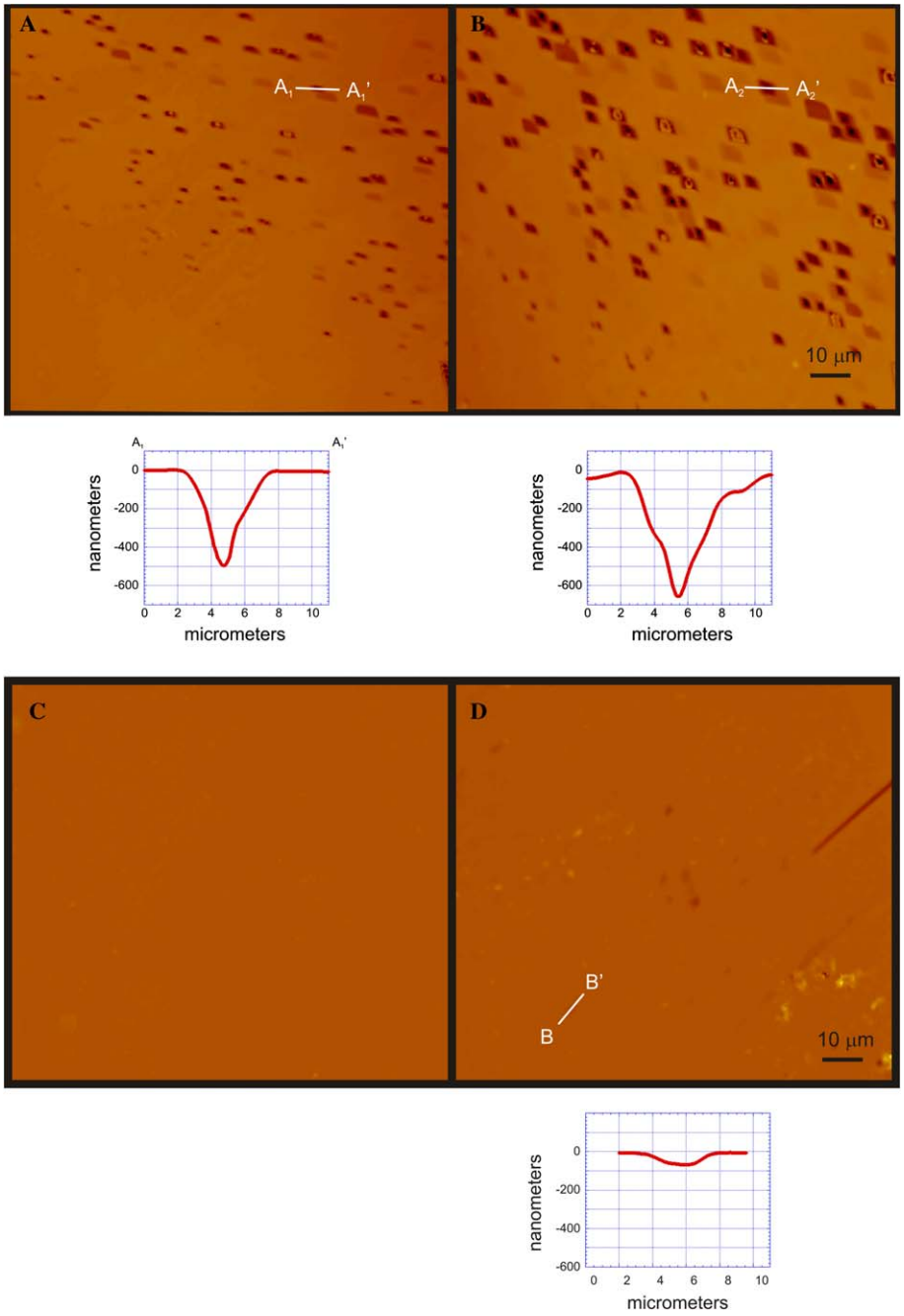


Fig. 8. Plane-view, shaded height maps of treated (upper) and untreated (lower) cleavage surfaces. (A) Treated sample with existing etch pits. (B) Identical surface after 149 h of dissolution at pH 9, 185 °C and −10.9 kJ/mol. (C) Untreated sample surface free of dissolution features. (D) Untreated sample after 149 h of dissolution at pH 9, 185 °C and −10.9 kJ/mol. The cross-sections under (A) and (B) show the development of the same etch pit during the experiment. The volume of albite removed by etch pit growth was $2.8 \times 10^{10}$ nm$^3$. The cross-section under (D) illustrates the size of a nascent etch pit on the reacted, non-pretreated sample. The volume removed by the formation of this etch pit was $3.4 \times 10^{8}$ nm$^3$.

SEM, in addition to VSI. In general, the crystal surfaces reacted at larger degrees of undersaturation showed a significantly higher etch pit density than crystal surfaces reacted nearer to equilibrium (compare Fig. 8A with Figs. 9 and 10). However, due to significant etch pit coalescence on samples reacted at $\Delta G_r \leqslant -29.3$ kJ/mol, etch pit densities on those surfaces were not quantified. In addition to a general decrease in pit density, we observed a strong decrease in the number of pyramidal pits as equilibrium was approached. One exception to this general observation was one experiment conducted at −10.2 kJ/mol.

### 3.2.3. Etch pit morphologies

On the samples reacted at $\Delta G_r \leqslant -20.5$ kJ/mol etch pits were elongated, crystallographically oriented rhombs. In general, the degree of elongation increased with decreasing albite saturation. The "short" sides of etch pits were parallel to the (010) cleavage faces. The angles created by the

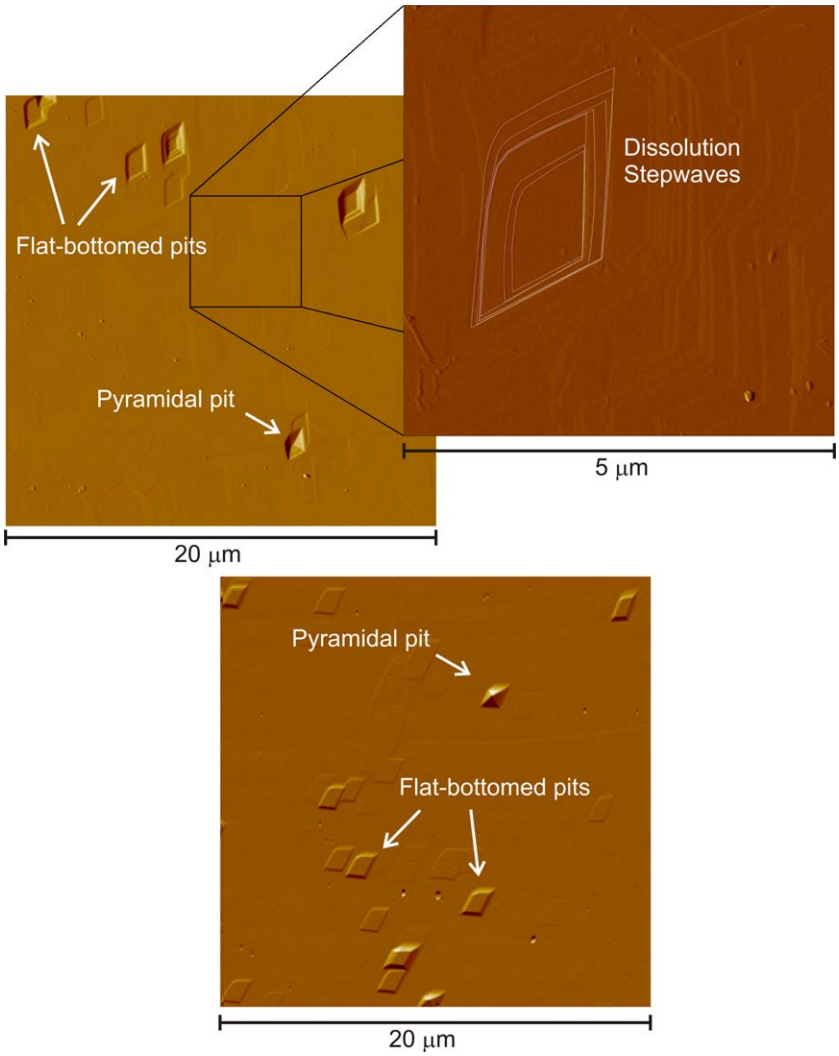


Fig. 9. AFM images of the untreated Greek albite (001) surface reacted for 99 h at $\Delta G_r = -14.5$ kJ/mol, pH 9 and 185 °C. Flat-bottomed etch pits dominate, although two pyramidal pits are visible. Inset shows a series of dissolution stepwaves surrounding shallow pits. Note the rounding of one corner of the pits.

intersection of the etch pit walls were approximately 60° and 120°. Etch pits on cleavage surfaces reacted at $\Delta G \leqslant -35.1$ kJ/mol exhibited rounding evident on one or two corners. Etch pits on surfaces reacted at −25.9 and −20.5 kJ/mol, in contrast, lacked any rounding. As was demonstrated in Fig. 8, etch pits on the pretreated crystal surface grew larger after further dissolution, yet maintained their lateral morphology. Etch pits with both pyramidal and flat bottoms were present.

During experiments conducted at $\Delta G_r \geqslant -14.5$ kJ/mol it was necessary to examine the reacted untreated cleavage surfaces using AFM or SEM, because the widths of etch pits ($\leqslant$1.5 μm) were close to the lateral resolution of VSI. Due to imaging artifacts at these conditions, pits appeared to be cone-shaped rather than euhedral. AFM and SEM imaging revealed rhomb-shaped, crystallographically controlled etch pits on all samples. Both pyramidal and flat-bottomed etch pits were present, although the number of pyramidal pits was lower than on samples from the far-from-equilibrium experiments. The high lateral and vertical resolution of the AFM allowed us to see very shallow (~8 nm), flat-bottomed pits dominating the reacted surfaces. Note the concentric steps around the vicinal faces of these pits that are visible in the AFM images of the non-pretreated surface reacted at $\Delta G = -12.3$ kJ/mol (shown here as an example in Fig. 10). The rounding of one corner of the etch pits is evident on all reacted albite surfaces, and can be observed in Figs. 8 and 9. This phenomenon may be analogous to the explanation for calcite etch pit morphologies given in, e.g., Arvidson et al., 2005.

The SEM photograph in Fig. 11A shows that dissolution at step edges inherited during the cleaving process contribute significantly to the overall dissolution rate. This is evident in the jagged nature of the step edges. The step edge in Fig. 11B was protected from dissolution by the mask and appears smooth in contrast. In the SEM images, the untreated surface reacted at a value of $\Delta G = -10.9$ kJ/mol show rounding on one corner and appear to be predominantly flat bottomed (Fig. 11C).

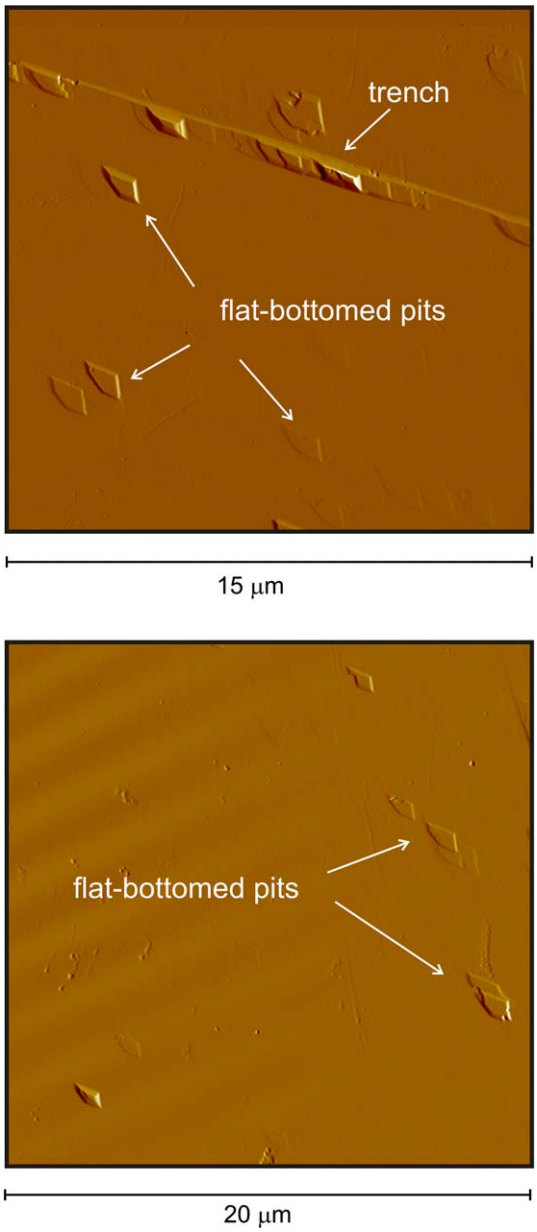


Fig. 10. AFM images of the untreated Greek albite (001) surface reacted for 144 h at $\Delta G_r = -12.3$ kJ/mol, pH 9 and 185 °C. Flat-bottomed etch pits dominate the surface. Top image exhibits a dissolution "trench" characterized by a locally higher pit density.

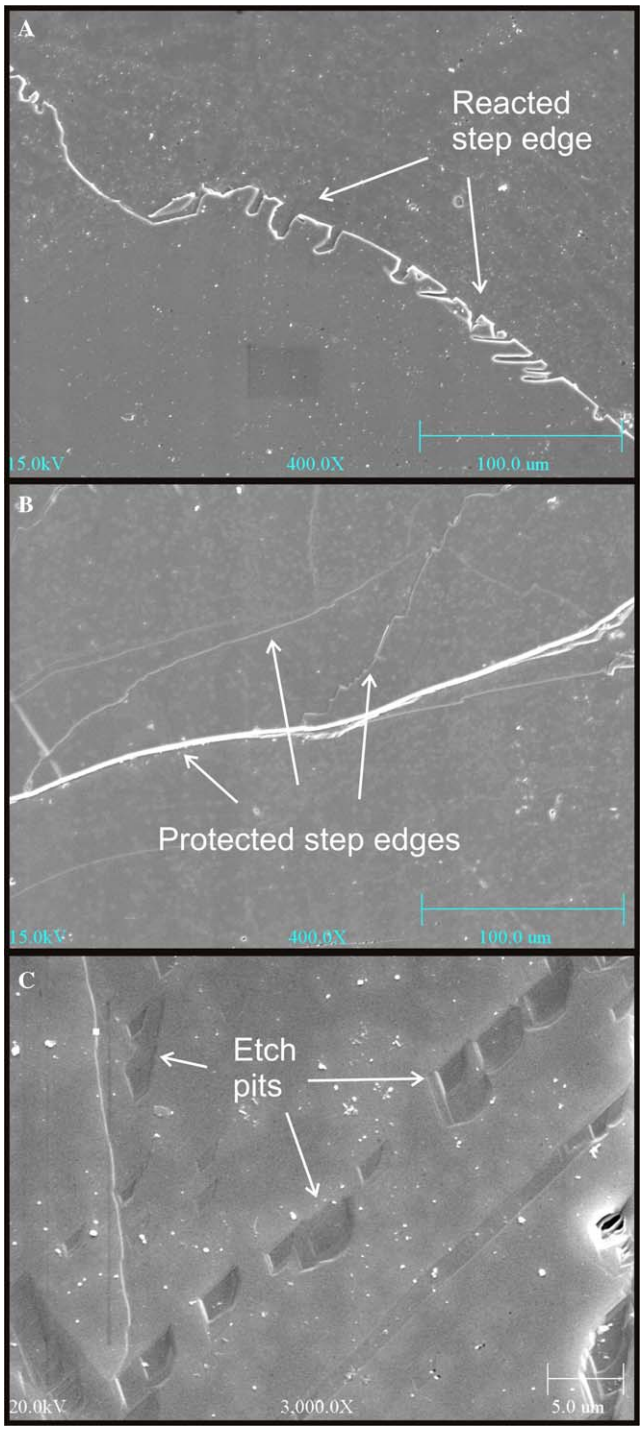


Fig. 11. SEM photomicrographs of the untreated Greek albite (001) surface reacted for 149 h of reaction at $\Delta G_r = -10.9$ kJ/mol, pH 9 and 185 °C. (A) Step edge inherited during cleaving process exhibits significant dissolution. (B) A similar step edge that had been protected during reaction by the Viton mask. (C) Reacted surface exhibiting flat-bottomed etch pits with significant rounding of one corner.

The non-pretreated surface reacted closest to equilibrium (−10.2 kJ/mol) exhibited rhomb-shaped pits lacking any rounding. Relative to the other near-equilibrium experiments, this reacted cleavage surface exhibited a higher number of pyramidal etch pits. However, etch pit densities were still much lower than on the samples reacted at $\Delta G \leqslant -20.5$ kJ/mol.

## 4. Discussion

Examination of the albite dissolution data from powder experiments of Burch et al. (1993, Fig. 1a) and labradorite dissolution data of Taylor et al. (2000, Fig. 1b) reveals a significant gap in dissolution rates with rates corresponding to Gibbs free energies <−35 kJ/mol approximately 5–50 times faster than the rates measured closer to equilibrium. Figs. 2A and B contain sketches representing two different dissolution mechanisms with different free energy depen-

dencies drawn over the plots of Burch et al. (1993) and Taylor et al. (2000). The sketches are drawn such that rates corresponding to Gibbs free energies <−35 kJ/mol fall upon the exponential curve (“fast” mechanism), while rates measured at Gibbs free energies >−35 kJ/mol fall upon the linear curve (“slow” mechanism). The lack of intermediate rates in both experiments can be interpreted as a discontinuity or “jump” in rate caused by the change from one governing reaction mechanism to another as the systems deviate from equilibrium. Making use of a simple analogy, consider two pumps with very different pumping rates. Pump A provides fluid at a rate of 10 U/time while pump B provides fluid at a rate of 10,000 U/time. Initially, only pump A is operating. As soon as pump B is switched on the contribution of pump A is immediately overwhelmed and the combined pumping rate would be 10,010 U/time. As steady state must be established first, we would expect to observe a similar behavior for crystals that experience a change from a slow to a significantly faster dissolution mechanism. That means we would not expect to measure any steady-state dissolution rates between 10 and 10,010 U/time at any point in time. If this scenario is valid, it would have far-reaching implications for any attempt to extrapolate far-from-equilibrium experimental data to near-equilibrium conditions.

Burch et al. (1993) and Taylor et al. (2000) attribute the dramatic increase in dissolution rates for values of $\Delta G < -35$ kJ/mol to the opening of etch pits on the crystal surfaces. Their conclusion is consistent with BCF theory and the model of Lasaga and Lüttge (2001, 2003) within which the opening of pits creates a new source for steps that was not present before. Recent in situ AFM studies have imaged dissolution stepwaves emanating from etch pits in calcite (Arvidson et al., 2005; Vinson and Lüttge, 2005). Ex situ AFM images from our study (Fig. 9 inset) show a series of what we interpret to be dissolution stepwaves surrounding shallow etch pits on the (001) cleavage surface of the Greek albite. Even if we were to disregard the stepwave model, the excavation at etch pits would be an effective additional mechanism for the removal of material and would thereby influence the dissolution rate significantly. An understanding of the cause of the “switch” in mechanism with deviation from equilibrium requires insight into the relationship between etch pit formation and Gibbs free energy.

According to accepted theory, etch pits form where, for example, line defects, such as screw dislocations, originating within the crystal lattice intersect its surface. Historically, the importance of dislocations in crystal growth was addressed by Frank (1951) and Burton et al. (1951) in their BCF crystal growth theory. BCF theory predicts that screw dislocations with sufficiently long Burgers vectors exhibit a “hollow core”. Cabrera et al. (1954) and Cabrera and Levine (1956) extended this theory to include crystal dissolution at screw dislocations. This theory relates the behavior of hollow cored dislocations to the Gibbs free energy of the solution. The relationship is expressed in Eq. (3) that predicts the critical undersaturation required to open the hollow core into an etch pit during dissolution:

$$RT\ln(C_{\mathrm{crit}}/C_0) = -2\pi^2\sigma^2\overline{V}/\mu b^2, \tag{2}$$

where $C_{\mathrm{crit}}$ is the critical concentration, $C_0$ is the equilibrium concentration, $\sigma$ is the surface free energy, $\overline{V}$ is the molar volume, $R$ is the gas constant, $T$ is the temperature, $\mu$ is the bulk shear modulus, and $b$ is the length of the Burgers vector. For undersaturations greater than $\ln(C_{\mathrm{crit}}/C_0)$, the hollow core is forced to open up and will form a macroscopic etch pit.

Similarly, the stepwave model predicts a critical undersaturation requirement ($\Delta G_{\mathrm{crit}}$) for the opening of etch pits (Lasaga and Lüttge, 2001, 2003)

$$\Delta G_{\mathrm{crit}} = -\sigma\overline{V}/r_{\mathrm{pit}} + u(r_{\mathrm{pit}})\overline{V}, \tag{3}$$

where $\sigma$ is the surface free energy, $\overline{V}$ is the molar volume, $r_{\mathrm{pit}}$ is the radius at which the velocity of the stepwaves reach a minimum, and $u(r_{\mathrm{pit}})$ is the strain energy at $r_{\mathrm{pit}}$. An abrupt switch from an etch-pit-free to an etch-pit-dominated mechanism should occur at $\Delta G_{\mathrm{crit}}$ (Lasaga and Blum, 1986; Brantley et al., 1986; Nagy and Lasaga, 1992; Burch et al., 1993; Taylor et al., 2000; Lasaga and Lüttge, 2001, 2003).

The kinetic behavior of single crystals may not be as clearly defined as that of mineral powders, the rates of which are an integration of the dissolution rates of all of the surfaces sites on a statistically large number of grains. Careful examination of the rate data and surface images of the untreated samples (squares, Fig. 7) from this study reveal some distinct similarities to, as well as differences from the “two-mechanism” datasets mentioned above. An important similarity is the existence of a near-equilibrium rate “plateau” in our data (Fig. 7), as well as those of Burch et al. (1993) and Taylor et al. (2000). The reacted cleavage surfaces in our study that exhibit a relatively weak dependence of dissolution rate on $\Delta G_{\mathrm{r}}$ and extremely slow dissolution rates are characterized by isolated, shallow, flat-bottomed pits (Figs. 9 and 10). The steep walls and flat bottoms of these pits make them ineffective at removing material, because of the tendency for step bunching. As can be seen in Fig. 11A, however, dissolution continues to occur at step edges, albeit slowly. Another similarity with the existing datasets is a sharp increase in dissolution rate with deviation from equilibrium. In our case, this first occurs somewhere between −16 and −20 kJ/mol, and is an increase of approximately one order of magnitude. We interpret the $\Delta G_{\mathrm{crit}}$ to lie somewhere in this range as indicated by the shaded region in Fig. 7. Beginning at −20.1 kJ/mol the slope of the untreated samples increases dramatically, defining a second region dominated by another dissolution mechanism. These reacted, untreated cleavage surfaces are characterized by abundant, coalescing pits hundreds of nanometers deep, such as those shown in Fig. 6. Unlike the data of Burch et al. (1993) and Taylor et al. (2000), our untreated data points exhibit a third region with an even stronger dependence of dissolution rate

on $\Delta G_r$. Again, these surfaces are characterized by abundant, deep pits with a greater degree of coalescence. Clearly, regions 2 and 3 in Fig. 7 represent dissolution dominated by localized removal of material at etch pits, as well as significant removal by stepwaves as indicated by the 25–380 nm of surface normal retreat exhibited by those samples.

In contrast to the untreated samples, the treated samples exhibit significant scatter (triangles, Fig. 7). Regions 1 and 2 show an enhancement in the dissolution rates of treated samples relative to the untreated samples reacted under identical conditions. The treated samples were etched at pH 9, 185 °C, and $\Delta G_r < 50$ kJ/mol (Region 3 conditions) and were characterized by abundant pits hundreds of nanometers deep. These treated samples benefited from a head start in stepwave production relative to the corresponding untreated samples. The convergence of rates between the treated and untreated samples at −61.1 kJ/mol indicates that pits effectively opened instantaneously on the untreated sample allowing excavation at pits and production of stepwaves to dominate the dissolution rate immediately. We expect that given sufficient time, the rates of treated and untreated samples in Region 2 would also converge. Our expectation is that the rates of the untreated samples would increase to those of the treated samples. However, the near convergence of rates at −20.1 kJ/mol seems to indicate otherwise. Of the three sample pairs in Region 2, the samples at −20.1 kJ/mol were reacted for the longest duration. It appears that although the dissolution mechanisms of Region 2 and 3 are similar, they exhibit different free energy dependencies.

Of particular importance to this study are the differences in dissolution rate between the treated and untreated sample pairs reacted closer to equilibrium than our interpreted $\Delta G_{crit}$. The treated samples in this free energy range are dissolving by a mechanism not stable in that region. In essence they represent a temporary, non-steady-state scenario. If dissolution were to occur long enough such that the existing deep pits were exhausted and the surface morphologies returned to that of the untreated samples, the rates of the treated samples would eventually drop onto the near-equilibrium plateau.

As outlined, the primary goal of our study was to elucidate the cause of the apparent differences in dissolution kinetics between experimental data collected in different laboratories. While some controversy may exist over the appropriate application of dissolution rate laws (e.g., TST-based rate laws to overall processes), the data collected by individual laboratory groups are internally consistent and not in question. Therefore, another explanation must exist for the apparent discrepancies between datasets.

In the following discussion, we present two different scenarios of an albite/water system undergoing dissolution. Both scenarios are consistent with experimental methods used and observations and measurements obtained by us and other investigators. This discussion will provide insight into some key differences in the reaction kinetics of mineral/fluid systems. Let us first consider the albite/water system when it is initially closer to equilibrium than the $\Delta G_{crit}$. Under the likely assumption that the crystal contains screw dislocations, hollow cores are already present, but they have not opened yet into etch pits. Therefore, the system must rely mainly on dissolution at cleavage steps and crystal edges. In our experiments, this case is represented by the untreated samples located right of the grey bar in Fig. 7. This reaction mechanism is inefficient because flat areas of the surface remain largely non-reactive and results in slow dissolution rates which exhibit a shallow, linear dependency on Gibbs free energy. If the system is driven further away from equilibrium, such that the $\Delta G_{crit}$ is reached, etch pits will open (samples left of the grey bar in Fig. 7). The opening of etch pits is caused by localized accelerated material removal. This new mechanism results in a more or less significant increase in dissolution rate. If we follow the reasoning of the stepwave model (Lasaga and Lüttge, 2001, 2003) the freshly opened pits provide an additional source for steps resulting in stepwaves causing a dramatic increase in dissolution rate. Note that the etch pits themselves which are formed at screw dislocations can be interpreted as the result of time integral over locally rapid step movement.

While the above scenario explains the bimodal reaction pathway observed in the data of such investigators as Nagy et al. (1991), Nagy and Lasaga (1992), Burch et al. (1993), Alekseyev et al., 1997, Taylor et al. (2000), and Berger et al. (2002), it does not explain the exponential or linear relationships observed in the data of Gautier et al. (1994), Oelkers et al. (1994), Devidal et al. (1997), and Oelkers and Schott (1999). An entirely different scenario is necessary to explain the rate dependency described by a single, continuous, exponential function. In this scenario the albite/water system is reacting initially far from equilibrium (i.e., on the dissolution plateau). Under these conditions etch pits open almost immediately. In our experiments this case is represented by the treated samples (Figs. 6 and 8A). Now, we drive this system toward equilibrium (again assuming that steady state is always established) until the $\Delta G_{crit}$ is surpassed. In contrast to the first scenario during which the kinetics were controlled by the slow, pit-free mechanism, the pits are still open and remain productive in generating stepwaves. In addition, increased mass removal at the pits themselves remains an important factor for the dissolution rate. That means the overall dissolution rate is still controlled by the fast, stepwave-driven mechanism. At this point the system can develop in one of two ways: (a) the approach to equilibrium is rapid and etch pits remain active the entire way to equilibrium, simulating a quasi-steady-state situation and (b) the approach to equilibrium is slow enough such that the active pits are removed before equilibrium is reached. In case (a) the presence of productive etch pits during the entire approach to equilibrium maintains the system on the fast, stepwave-dominated curve (Fig. 2C) In case (b), after a sufficient length of time closer to equilibrium than $\Delta G_{crit}$, the etch

pits would begin to disappear as their dislocations jogged or were intersected, and stepwaves continue to remove layers of material around them. As long as the environmental conditions remained closer to equilibrium than $\Delta G_{crit}$, they would not be replaced by new etch pits as new dislocations were unearthed. Eventually, the system is forced from the exponential or linear path of the fast mechanism onto the shallow, linear graph that represents the slow mechanism. Case (a) seems consistent with the dissolution behavior observed in the experimental data of Oelkers et al. (1994) and Gautier et al. (1994). As stated earlier, their data exhibit an exponential dependence of dissolution rate on Gibbs free energy. Because the experiments of Oelkers et al. (1994) were initiated far from equilibrium (Oelkers, personal communication), they most likely measured the Gibbs free energy dependency of the fast (stepwave dominated) dissolution mechanism (Fig. 2C). Case (b) represents an alternative reaction pathway for achieving a bimodal data distribution similar to those of Burch et al. (1993) and Taylor et al. (2000). A third, intermediate situation may exist between case (a) and (b). A number of datasets are compatible with a sigmoidal dependence of dissolution rate on free energy, yet exhibit intermediate rates between those of the fast, pit-dominated mechanism and the slow, step-dominated mechanism (Alekseyev et al., 1997; Berger et al., 2002). Given that the data of Alekseyev et al., Berger et al. exhibit sigmoidal relationships between rate and free energy, we do not consider them to be in contradiction to our proposed model. It is possible that the presence of intermediate rates is the result of etch pits remaining on a portion of the powder grains. If experiments at $\Delta G_r > \Delta G_{crit}$ were run until the etch pits were exhausted on all grains, the rates may have decreased onto the near-equilibrium plateau.

## 5. Implications for natural and experimental systems

Let us revisit case (b) from above. Based upon our rate measurements, it would take approximately $2 \times 10^6$ years of dissolution to produce 10 nm of surface-normal retreat on the (001) cleavage surface of albite dissolving at pH 3 and 25 °C. At those conditions it could take tens of millions of years for the etch pits to be removed. It is entirely possible that in the case of a slowly dissolving mineral such as albite, the approach to equilibrium would occur more quickly. Such a system would, therefore, be dominated by the stepwave mechanism for its entire history. In contrast, highly reactive minerals, such as calcite, could deviate relatively quickly from their temporary non-steady state and experience a mechanistic switch in a much shorter amount of time.

Mineral/fluid systems in nature are subject to even further complexity. It is likely that for any given field scenario we could measure a range of dissolution rates between those predicted by the two-mechanisms illustrated in Fig. 2. For example, take a natural mineral/fluid system containing crystals from a variety of sources. If the histories of the source materials were different, some crystals may exhibit preexisting etch pits while other would not. A high solid to fluid ratio, a common scenario in subsurface aquifers, could result in the system being closer to equilibrium than $\Delta G_{crit}$. In this case, the overall dissolution rate of the system would consist of contributions from crystals dominated by both the slow and fast mechanisms. As a result we would measure an overall dissolution rate somewhere in between those predicted by either mechanism.

## 6. Summary and conclusions

We quantified the dissolution rates of and identified the reaction mechanisms on albite crystal surfaces over a wide range of Gibbs free energy. We have measured an approximately 1–2 order of magnitude difference in dissolution rate between treated and untreated sample pairs. Examination of the crystal surfaces post-reaction indicates that the dissolution kinetics of albite crystals that have experienced different histories are dominated by different dissolution mechanisms. Each mechanism exhibits a different Gibbs free energy dependency resulting eventually in a kinetic discontinuity as conditions deviate from equilibrium. Depending on the crystallography, dislocation types, and dislocation density this scenario can result in a more or less pronounced gap of dissolution rates, such as those observed by Burch et al. and Taylor et al. Our experimental results point toward the existence of such a gap as well. However, since VSI data represent time integrated surface-normal retreat rates, non-steady state rates are included in the integration. Therefore, our data are somewhat smeared and not specific enough to exclude other possible explanations. More work is necessary to decide this question distinctively. Despite this caveat, and even if no rate gap would be present, at least two different rate laws are necessary to appropriately describe the dissolution kinetics. This conclusion is consistent with other recent experimental data for albite dissolution kinetics obtained by Hellmann and Tisserand (2006).

Our observations provide insight into the origins of and a possible explanation for the discrepancies in rate data generated by different laboratories for similar mineral/fluid systems. The direction in which experiments proceed, i.e., beginning near equilibrium and moving away from or beginning on the dissolution plateau and moving toward equilibrium, can control the resulting dependency of dissolution rate on Gibbs free energy. Experiments initiated near-equilibrium and subsequently driven away from equilibrium result in a rate gap caused by the change from a pit-free to a pit-dominated dissolution mechanism. This result implies that a mineral sample's reaction history can have a significant impact on its subsequent dissolution rate. In natural systems with slower overall rates and interrupted wetting conditions, this effect is likely to be even more pronounced. The consequence of such a scenario is the existence of a range of dissolution rates at a given set of otherwise identical environmental parameters.

**Acknowledgments**

The authors thank Rolf S. Arvidson, Tom A. Fewless, Michael D. Vinson, Kevin J. Davis, Li Zhang, and Catherine M. Cooper for their thoughtful comments and helpful discussion. We also thank Tom A. Fewless for performing the SEM work, Rolf S. Arvidson for assistance in performing the AFM work, and Alexis Offner for her help with the spectrophotometric analyses. A special thanks goes to Eberhard Seidel for providing the Greek albite samples along with valuable information on the sample material. We also thank three anonymous reviewers whose thoughtful comments were extremely helpful in improving this manuscript. We gratefully acknowledge funding for this study from the Department of Energy Grant # DE-FG07-01ER63295, the National Science Foundation Grant # EAR-0125667, the Mineralogical Society of America Edward H. Kraus Crystallographic Research Fund, and Rice University.

*Associate editor:* David J. Wesolowski

**Appendix A**

Summary of Si and Al concentrations over time. The average $\Delta G_r$ values reported in Table 2 were calculated using negative values of $\Delta G_r$ only, as this is the range in which dissolution is possible

| Time elapsed (h) | Si (mol/L) | Al (mol/L) | $T$ (±1 °C) | $\Delta G$ (kJ/mol) |
|---|---|---|---|---|
| *Ab12 A2 and B* | | | | |
| 21.8 | 0.000033 | 0.000024 | 185 | −58.8 |
| 23.5 | 0.000031 | 0.000019 | 185 | −59.8 |
| 45.9 | 0.000027 | 0.000014 | 185 | −62.8 |
| 48.9 | 0.000028 | 0.000015 | 185 | −61.9 |
| 50.2 | 0.000027 | 0.000014 | 185 | −62.8 |
| 69.4 | 0.000028 | 0.000016 | 185 | −61.5 |
| 73.7 | 0.000030 | 0.000022 | 185 | −59.8 |
| *Ab07 B1* | | | | |
| 20.0 | 2.48273E−05 | 0.000137 | 185 | −54.89 |
| 44.0 | 2.43823E−05 | 0.000133 | 185 | −55.19 |
| *Ab09 A1* | | | | |
| 42.0 | 4.44E−05 | 5.19E−05 | 185 | −51.97 |
| *Ab10 A1* | | | | |
| 1.2 | 0.000021 | 4.00E−05 | 173 | −57.74 |
| 3.4 | 0.000115 | 6.53E−05 | 173 | −36.94 |
| 4.9 | 0.000194 | 8.43E−05 | 185 | −33.22 |
| 23.8 | 0.000192 | 8.58E−05 | 185 | −33.30 |
| 29.3 | 0.000275 | 1.16E−04 | 185 | −27.99 |
| 30.3 | 0.000276 | 1.16E−04 | 185 | −27.95 |
| 47.9 | 0.000166 | 7.82E−05 | 185 | −35.31 |
| 53.0 | 0.000205 | 9.31E−05 | 185 | −32.22 |
| 73.4 | 0.000174 | 8.34E−05 | 185 | −34.52 |
| 76 | 0.000206 | 9.22E−05 | 185 | −32.22 |
| *Ab13 A2 and B* | | | | |
| 0 | 0.000199 | 7.57E−05 | 179 | −31.8 |
| 0.8 | 0.000327 | 0.000103 | 201 | −30.1 |
| 16.5 | 0.000367 | 0.000105 | 185 | −25.1 |
| 19.1 | 0.000277 | 0.000102 | 185 | −28.5 |
| 20.3 | 0.000367 | 0.000101 | 185 | −25.1 |
| 39.2 | 0.000263 | 9.38E−05 | 185 | −29.3 |
| 43.9 | 0.000265 | 9.53E−05 | 185 | −29.3 |
| 63.7 | 0.000257 | 9.21E−05 | 185 | −29.7 |
| 67.2 | 0.000254 | 9.13E−05 | 185 | −29.7 |
| 69.4 | 0.000257 | 9.34E−05 | 185 | −29.7 |
| 87.7 | 0.000252 | 9.19E−05 | 185 | −29.7 |
| 89.7 | 0.000253 | 9.06E−05 | 185 | −29.7 |
| 93.3 | 0.000258 | 8.89E−05 | 185 | −29.7 |
| 111.4 | 0.000244 | 8.89E−05 | 185 | −30.5 |
| 115.2 | 0.000248 | 8.87E−05 | 185 | −30.1 |
| 117.2 | 0.000253 | 9.17E−05 | 185 | −29.7 |
| 135.9 | 0.000257 | 8.85E−05 | 185 | −29.7 |
| 137.5 | 0.000259 | 8.69E−05 | 185 | −29.7 |
| *Ab10 A2 and B* | | | | |
| 2.5 | 0.000068 | 0.000033 | 188 | −49.71 |
| 20.8 | 0.000428 | 0.000227 | 185 | −20.33 |
| 24.2 | 0.000433 | 0.000192 | 185 | −20.84 |
| 25.7 | | 0.000203 | 185 | |
| 43.1 | 0.000479 | 0.000208 | 185 | −19.37 |
| 68.8 | 0.000365 | 0.000193 | 185 | −22.76 |
| 94.2 | 0.000440 | 0.000281 | 185 | −19.16 |
| 97.2 | 0.000387 | 0.000309 | 185 | −20.25 |
| 115.8 | 0.000397 | 0.000141 | 185 | −23.01 |
| 120.9 | 0.000381 | 0.000132 | 185 | −23.77 |
| 141.3 | 0.000367 | 0.000119 | 185 | −24.60 |
| 143.5 | 0.000323 | 0.000119 | 185 | −26.07 |
| 164.3 | 0.000219 | 0.000077 | 185 | −32.17 |
| 166.2 | 0.000233 | 0.000088 | 185 | −30.96 |
| 168.0 | 0.000240 | 0.000101 | 185 | −30.08 |
| *Ab08 A2 and B* | | | | |
| 0.9 | 0.000158 | 0.000106 | 95 | 4.6 |
| 4.8 | 0.000265 | 0.000119 | 71 | −8.4 |
| 5.3 | 0.000388 | 0.000128 | 185 | 3.3 |
| 17.3 | 0.000651 | 0.000172 | 185 | −26.8 |
| 19.8 | 0.000659 | 0.000162 | 185 | −16.7 |
| 21.9 | 0.000675 | 0.000278 | 185 | −14.6 |
| 24.1 | 0.000648 | 0.000174 | 185 | −15.9 |
| 29.2 | 0.000501 | 0.000118 | 185 | −18.0 |
| 41.3 | 0.000431 | 0.000118 | 185 | −20.9 |
| 46.4 | 0.000391 | 0.000093[a] | 185 | −24.7[b] |

(*continued on next page*)

**Appendix A** (*continued*)

| Time elapsed (h) | Si (mol/L) | Al (mol/L) | $T$ (±1 °C) | $\Delta G$ (kJ/mol) |
|---|---|---|---|---|
| 48.3 | 0.000428 | 0.000102[a] | 185 | −23.4[b] |
| 65.8 | 0.000424 | 0.000100[a] | 185 | −23.4[b] |
| 71.3 | 0.000315 | 0.000075[a] | 185 | −28.0[b] |
| *Ab09 A2 and B* | | | | |
| 2.4 | 0.000331 | | 140 | |
| 2.8 | 0.000360 | 0.000076 | 168 | −20.9 |
| 4.0 | 0.000516 | 0.000099 | 185 | −19.2 |
| 9.1 | 0.000830 | 0.000129 | 185 | −11.7 |
| 21.2 | 0.000879 | 0.000193 | 185 | −10.9 |
| 24.2 | 0.001197 | 0.000135 | 185 | −6.2 |
| 27.7 | 0.001121 | 0.000139 | 185 | −7.5 |
| 31.8 | 0.000695 | 0.000218 | 185 | −14.6 |
| 45.2 | 0.000645 | 0.000138 | 185 | −15.9 |
| 46.4 | 0.000646 | | 185 | |
| 49.4 | 0.000626 | 0.000200 | 185 | −16.3 |
| 56.6 | 0.000672 | | 185 | |
| 67.7 | 0.000615 | | 185 | |
| 70.7 | 0.000563 | | 185 | |
| 78.0 | 0.000608 | 0.000454 | 185 | −16.7 |
| 90.5 | 0.000605 | 0.000535 | 185 | −16.7 |
| 98.9 | 0.000570 | 0.000493 | 185 | −17.6 |
| *Ab06 A2 and B* | | | | |
| 3.3 | 0.000658 | | 85 | |
| 17.5 | 0.000943 | 0.000423 | 190 | −9.75 |
| 48.3 | 0.000926 | 0.000345 | 185 | −9.75 |
| 69.5 | 0.000813 | 0.000384 | 185 | −10.84 |
| 88.8 | 0.000704 | 0.000319 | 185 | −13.26 |
| 94.3 | 0.000693 | 0.000304 | 185 | −13.60 |
| 118.3 | 0.000662 | 0.000269 | 185 | −14.64 |
| 142.3 | 0.000693 | 0.000259 | 185 | −14.23 |
| *Ab05 A2 and B* | | | | |
| 3.0 | 0.000331 | 0.000326 | 105 | −1.72 |
| 4.1 | 0.000343 | 0.000213 | 141 | −12.38 |
| 4.8 | 0.000415 | | 158 | |
| 7.8 | 0.000937 | 0.000329 | 185 | −9.83 |
| 20.1 | 0.000801 | 0.000358 | 185 | −11.30 |
| 22.9 | 0.000761 | 0.000360 | 185 | −11.88 |
| 25.0 | 0.000776 | 0.000271 | 185 | −12.76 |
| 44.0 | 0.000818 | | 185 | |
| 68.0 | 0.000861 | 0.000302 | 185 | −11.13 |
| 93.0 | 0.000803 | 0.000300 | 185 | −11.97 |
| 144.5 | 0.000825 | 0.000264 | 185 | −12.13 |
| 140.9 | 0.000841 | 0.000246 | 185 | −12.22 |
| 148.0 | 0.000788 | 0.000265 | 185 | −12.68 |
| *Ab11 B* | | | | |
| 1.1 | 0.001367 | 0.000450 | 100 | 14.1 |
| 2.3 | 0.001795 | 0.000569 | 190 | −6.6 |
| 8.6 | 0.001250 | 0.000414 | 185 | −5.6 |
| 22.0 | 0.001032 | 0.000231 | 185 | −10.1 |
| 24.1 | 0.000923 | 0.000329 | 185 | −10.0 |
| 25.6 | 0.000956 | 0.000301 | 185 | −9.9 |
| 27.1 | 0.000934 | 0.000267 | 185 | −10.8 |
| 45.4 | 0.000906 | 0.000326 | 185 | −10.8 |
| 47.9 | 0.000936 | 0.000359 | 185 | −10.3 |
| 51.4 | 0.000915 | 0.000331 | 185 | −10.0 |
| 69.0 | 0.000924 | 0.000360 | 185 | −9.7 |
| 72.0 | 0.000856 | 0.000259 | 185 | −11.7 |
| 73.1 | 0.000954 | 0.000262 | 185 | −10.6 |
| 75.7 | 0.000854 | 0.000258 | 185 | −11.9 |
| 91.7 | 0.000910 | 0.000286 | 185 | −10.7 |
| 94.7 | 0.000802 | 0.000290 | 185 | −12.1 |
| 118.7 | 0.000814 | 0.000323 | 185 | −11.6 |

[a] Estimate based upon [Si]/[Al] = 4.22 of measurement at 41.3 h.

[b] Based upon measured [Si] and estimated [Al]. Average $\Delta G_r$ presented in Table 2 includes these estimates.

## References


Alekseyev, V.A., Medvedeva, L.S., Prisyagina, N.I., Meshalkin, S.S., Balabin, A.I., 1997. Change in the dissolution rates of alkali feldspars as a result of secondary mineral precipitation and approach to equilibrium. *Geochim. Cosmochim. Acta* **61**, 1125–1142.

American Public Health Association, American Water Works Association, and Water Pollution Control Federation 1995. *Standard Methods for the Examination of Water and Wastewater*, 19th ed., method 4500-Si D, pp. 4–118.

Amrhein, C., Suarez, D.L., 1988. The use of a surface complexation model to describe the kinetics of ligand-promoted dissolution of anorthite. *Geochim. Cosmochim. Acta* **52**, 2785–2793.

Amrhein, C., Suarez, D.L., 1992. Some factors affecting the dissolution kinetics of anorthite at 25 °C. *Geochim. Cosmochim. Acta* **56**, 1815–1826.

Arvidson, R.S., Beig, M.S., Lüttge, A., 2004. Single-crystal plagioclase feldspar dissolution rates measured by vertical scanning interferometry. *Am. Mineral.* **89**, 51–56.

Arvidson, R.S., Collier, M., Davis, K.J., Vinson, M.D., Lüttge, A., 2005. Magnesium inhibition of calcite dissolution kinetics. *Geochim. Cosmochim. Acta.* **70**, 583–594.

Berger, G., Beaufort, D., Lacharpagne, J.-L., 2002. Experimental dissolution of sanidine under hydrothermal conditions: mechanism and rate. *Am. J. Sci.* **302**, 663–685.

Berner, R.A., Holdren Jr., G.R., 1979. Mechanism of feldspar weathering II. Observations of feldspars from soils. *Geochim. Cosmochim. Acta* **43**, 1173–1186.

Berner, R.A., Schott, J., 1982. Mechanism of pyroxene and amphibole weathering II. Observations of soil grains. *Am. J. Sci.* **282**, 1214–1231.

Brantley, S.L., Crane, S.R., Crerar, D.A., Hellmann, R., Stallard, R., 1986. Dissolution at dislocation etch pits in quartz. *Geochim. Cosmochim. Acta* **50**, 2349–2361.

Brantley, S.L., Stillings, L.L., 1996. Feldspar dissolution at 25 °C and low pH. *Am. J. Sci.* **296** (2), 101–127.

Burch, T.E., Nagy, K.L., Lasaga, A.C., 1993. Free energy dependence of albite dissolution kinetics at 80 °C and pH 8.8. *Chem. Geol.* **105**, 137–162.

Burton, W.K., Cabrera, N., Frank, F.C., 1951. The growth of crystals and the equilibrium structure of their surfaces. *Phil. Trans. R. Soc. Lond. Ser. A* **243**, 299–358.

Cabrera, N., Levine, M.M., 1956. On the dislocation theory of evaporation of crystals. *Phil. Mag.* **1**, 450–458.

Cabrera, N., Levine, M.M., Plaskett, J.S., 1954. Hollow dislocations and etch pits. *Phys. Rev.* **96**, 1153.

Casey, W.H., Carr, M.J., Graham, R.A., 1988a. Crystal defects and the dissolution kinetics of rutile. *Geochim. Cosmochim. Acta* **52**, 1545–1556.

Casey, W.H., Westrich, H.R., Arnold, G.W., 1988b. Surface chemistry of labradorite feldspar reacted with aqueous solutions at pH 2, 3, and 12. *Geochim. Cosmochim. Acta* **52**, 2795–2807.

Chou, L., Wollast, R., 1984. Study of the weathering of albite at room temperature and pressure with a fluidized bed reactor. *Geochim. Cosmochim. Acta* **48**, 2205–2217.

Chou, L., Wollast, R., 1985. Steady-state kinetics and dissolution mechanisms of albite. *American Journal of Science* **285** (December), 963–993.

Cygan, R.T., Casey, W.H., Boslough, M.B., Westrich, H.R., Carr, M.J., Holdren Jr., G.R., 1989. Dissolution kinetics of experimentally shocked silicate minerals. *Chem. Geol.* **78**, 229–244.

Devidal, J.-L., Schott, J., Dandurand, J.-L., 1997. An experimental study of kaolinite dissolution and precipitation kinetics as a function of chemical affinity and solution composition at 150 °C, 40 bars, and pH 2, 6.8, and 7.8. *Geochim. Cosmochim. Acta* **61** (24), 5165–5186.

Dougan, W.K., Wilson, A.L., 1974. The absorptiometric determination of aluminum in water. A comparison of some chromogenic reagents and the development of an improved method. *Analyst* **99**, 413–430.

Drake, B., Hellmann, R., 1991. Atomic force microscopy imaging of the albite (010) surface. *Am. Mineral.* **76**, 1773–1776.

Frank, F.C., 1951. Capillary equilibria of dislocated crystals. *Acta Crystallogr.* **4**, 497–501.

Ganor, J., Mogollon, J.L., Lasaga, A.C., 1995. The effect of pH on kaolinite dissolution rates and on activation energy. *Geochim. Cosmochim. Acta* **59**, 1037–1052.

Gautier, J.-M., Oelkers, E.H., Schott, J., 1994. Experimental study of K-feldspar dissolution rates as a function of chemical affinity at 150 C and pH 9. *Geochim. Cosmochim. Acta* **58** (21), 4549–4560.

Gíslason, S.R., Arnórsson, S., 1990. Saturation state of natural waters in Iceland relative to primary and secondary minerals in basalts. In: Spencer, R.J., Chou, I.M. (Eds.), *Fluid Mineral Interactions: A tribute to H.P. Eugster*. Geochemical Society Special Publication. pp. 373–393.

Helgeson, H.C., Murphy, W.M., Aargaard, P., 1984. Thermodynamic and kinetic constraints on reaction rates among minerals and aqueous solutions. II. Rate constants, effective surface area, and the hydrolysis of feldspar. *Geochim. Cosmochim. Acta* **48**, 2405–2432.

Harlow, G.E., Brown Jr., G.E., 1980. Low albite: an X-ray and neutron diffraction study. *Am. Mineral.* **65**, 986–995.

Hellmann, R., Drake, B., Kjoller, K., 1992. Using atomic force microscopy to study the structure, topography and dissolution of albite surfaces. In: Kharaka, Y.K., Maest, A.S. (Eds.), *Water Rock Interaction*. A.A. Balkema, pp. 149–152.

Hellmann, R., 1994. The albite-water system: Part I. The kinetics of dissolution as a function of pH at 100, 200, and 300 °C. *Geochim. Cosmochim. Acta* **58**, 595–611.

Hellmann, R., Tisserand, D., 2006. Dissolution kinetics as a function of the Gibbs free energy of reaction: an experimental study based on albite feldspar Part I. *Geochim. Cosmochim. Acta* **70**, 364–383.

Hochella Jr., M.F., Eggleston, C.M., Elings, V.B., Thompson, M.S., 1990. Atomic structure and morphology of the albite {010} surface: an atomic-force microscope and electron diffraction study. *Am. Mineral.* **75**, 723–730.

Holdren Jr., G.R., Berner, R.A., 1979. Mechanism of feldspar weathering I. Experimental studies. *Geochim. Cosmochim. Acta* **43**, 1161–1172.

Holdren Jr., G.R., Speyer, G.R., 1985a. Reaction rate-surface area relationships during the early stages of weathering I. Initial observations. *Geochim. Cosmochim. Acta* **49**, 675–681.

Holdren Jr., G.R., Speyer, P.M., 1985b. pH dependent changes in the rates and stoichiometry of dissolution of an alkali feldspar at room temperature. *Am. J. Sci.* **285**, 994–1026 (December).

Holdren Jr., G.R., Speyer, P.M., 1987. Reaction rate–surface area relationships during the early stages of weathering II. Data on eight additional feldspars. *Geochim. Cosmochim. Acta* **51**, 2311–2318.

Huang, W.-L., Longo, J.M., 1992. The effect of organics on feldspar dissolution and the development of secondary porosity. *Chem. Geol.* **98**, 271–292.

Knauss, K.G., Wolery, T.J., 1986. Dependence of albite dissolution kinetics on pH and time at 25 and 70 °C. *Geochim. Cosmochim. Acta* **50**, 2481–2497.

Lasaga, A.C., 1998. *Kinetic Theory and Applications in Earth Sciences*. Princeton Press, Princeton, NJ.

Lasaga, A.C., Blum, A.E., 1986. Surface chemistry, etch pits and mineral-water reactions. *Geochim. Cosmochim. Acta* **50**, 2363–2379.

Lasaga, A.C., Lüttge, A., 2001. Variation of crystal dissolution rate based on a dissolution stepwave model. *Science* **291**, 2000–2004.

Lasaga, A.C., Lüttge, A., 2003. A model for crystal dissolution. *Eur. J. Mineral.* **15**, 603–615.

Lüttge, A., 2004. Crystal dissolution kinetics studied by vertical scanning interferometry and Monte Carlo simulations: a brief review and outlook. In: Liu, X-Y., De Yoreo, J.J. (Eds.) *Nanoscale Structure and Assembly at Solid–Fluid Interfaces. Vol. I. Interfacial Structures versus Dynamics*. Series on Nanoscience and Technologies. Kluwer Academic Publisher, pp. 209–247.

Lüttge, A., Bolton, E.W., Lasaga, A.C., 1999. An interferometric study of the dissolution kinetics of anorthite: the role of reactive surface area. *Am. J. Sci.* **299**, 652–678.

Lüttge, A., Winkler, U., Lasaga, A.C., 2003. Dolomite dissolution kinetics studied with vertical scanning interferometry. *Geochim. Cosmochim. Acta* **67**, 1099–1116.

MacInnis, I.N., Brantley, S.L., 1992. The role of dislocations and surface morphology in calcite dissolution. *Geochim. Cosmochim. Acta* **56**, 1113–1126.

MacInnis, I.N., Brantley, S.L., 1993. Development of etch pit size distributions on dissolving minerals. *Chem. Geol.* **105**, 31–49.

Mast, M.A., Drever, J.L., 1987. The effect of oxalate on the dissolution rates of oligoclase and tremolite. *Geochim. Cosmochim. Acta* **51**, 2559–2568.

Merino, E., 1975. Diagenesis in Tertiary sandstones from Kettleman North Dome, California. II. Interstitial solutions: distribution of aqueous species at 100 °C and chemical relation to the diagenetic mineralogy. *Geochim. Cosmochim. Acta* **39**, 1629–1645.

Muir, I.J., Nesbitt, H.W., 1991. Effects of aqueous cations on the dissolution of labradorite feldspar. *Geochim. Cosmochim. Acta* **55**, 3181–3189.

Murphy, W.M., 1989. Dislocations and feldspar dissolution. *Eur. J. Mineral.* **1** (3), 315–326.

Nagy, K.L., Blum, A.E., Lasaga, A.C., 1991. Dissolution and precipitation kinetics of kaolinite at 80 C and pH 3: the dependence on solution saturation state. *Am. J. Sci.* **291** (September), 649–686.

Nagy, K.L., Lasaga, A.C., 1992. Dissolution and precipitation kinetics of gibbsite at 80 °C and pH 3: the dependence on solution saturation state. *Geochim. Cosmochim. Acta* **56**, 3093–3111.

Nesbitt, H.W., MacRae, N.D., Shotyk, W., 1991. Congruent and incongruent dissolution of labradorite in dilute, acidic, salt solutions. *J. Geol.* **99**, 429–442.

Oelkers, E.H., Schott, J., Devidal, J.-L., 1994. The effect of aluminum, pH, and chemical affinity on the rates of aluminosilicate dissolution reactions. *Geochim. Cosmochim. Acta* **58** (9), 2011–2024.

Oelkers, E.H., Schott, J., 1999. Experimental study of kyanite dissolution rates as a function of chemical affinity and solution composition. *Geochim. Cosmochim. Acta* **63** (6), 785–797.

Oxburgh, R., Drever, J.I., Sun, Y.-T., 1994. Mechanism of plagioclase dissolution in acid solution at 25 °C. *Geochim. Cosmochim. Acta* **58** (2), 661–669.

Pačes, T., 1972. Chemical characteristics and equilibration in natural water-felsic rock-CO2 systems. *Geochim. Cosmochim. Acta* **36**, 217–240.

Pačes, T., 1973. Steady-state kinetics and equilibrium between ground water and granitic rock. *Geochim. Cosmochim. Acta* **37**, 2641–2663.

Rose, N.M., 1991. Dissolution rates of prehnite, epidote, and albite. *Geochim. Cosmochim. Acta* **55**, 3273–3286.

Schweda, P., 1989. Kinetics of alkali feldspar dissolution at low temperature. *Water–Rock Interact. WRI-6*, 609–612.

Seidel, E., 1978. Zur Petrologie der Phyllit-Quarzit-Serie Kretas. Habilitation thesis, University Braunschweig, Germany.

Seidel, E., Kreuzer, H., Harre, W., 1982. A late oligocene/early Miocene high pressure belt in the external Hellenides. *Geol. Jahrb.* **E23**, 165–206.

Stillings, L.L., Brantley, S.L., 1995. Feldspar dissolution at 25 °C and pH 3: reaction stoichiometry and the effect of cations. *Geochim. Cosmochim. Acta* **59** (8), 1483–1496.

Stillings, L.L., Drever, J.I., Brantley, S.L., Sun, Y., Oxburgh, R., 1996. Rates of feldspar dissolution at pH 3–7 with 0–8 mM oxalic acid. *Chem. Geol.* **132**, 79–89.

Stoessel, R.K., Pittman, E.D., 1990. Secondary porosity revisited: the chemistry of feldsapr dissolution by carboxylic acids and anions. *Am. Assoc. Petrol. Geol. Bull.* **74**, 1795–1805.

Talman, S.J., Nesbitt, H.W., 1988. Dissolution of populations of ultrafine grains with applications to feldspars. *Geochim. Cosmochim. Acta* **52**, 1467–1471.

Tang, R., Nancollas, G.H., 2000. Abnormal dissolution of octacalcium phosphate crystals at constant undersaturation. *J. Crystal Growth* **212**, 261–269.

Tang, R., Nancollas, G.H., Orme, C.A., 2001. Mechanism of dissolution of sparingly soluble electrolytes. *J. Am. Chem. Soc.* **123**, 5437–5443.

Tang, R., Orme, C.A., Nancollas, G.H., 2003. A new understanding of demineralization: the dynamics of brushite dissolution. *J. Phys. Chem. B* **107**, 10653–10657.

Taylor, A.S., Blum, J.D., Lasaga, A.C., 2000. The dependence of labradorite dissolution and Sr isotope release rates on solution saturation state. *Geochim. Cosmochim. Acta* **64** (14), 2389–2400.

Vinson, M.D., Lüttge, A., 2005. Multiple length-scale kinetics: an integrated study of calcite dissolution rates and strontium inhibition. *Am. J. Sci.* **305**, 119–146.

White, A.F., Brantley, S.L., 2003. The effect of time on the weathering of silicate minerals: why do weathering rates differ in the laboratory and the field? *Chem. Geol.* **202**, 479–506.

White, A.F., Peterson, M.L., 1990. Role of reactive-surface-area characterization in geochemical kinetics models. In: Melchior, D.C., Bassett, R.L. (Eds.), *Chemical Modeling of Aqueous Systems II*, vol. 416, pp. 461–475.

Wolery, T.J., 1983. EQ3NR. *A Computer Program for Geochemical Aqueous Speciation-solubility Calculations: User's Guide and Documentation*. Lawrence Livermore National Laboratory, pp. 191.